annalen der physik
www.ann-phys.org

Lateral Photovoltaic Effect and Photo-Induced Resistance Effect in Nanoscale Metal-Semiconductor Systems

*Anhua Dong and Hui Wang**

Functionalization of photoelectric effect in nanostructures is presenting a promising strategy for humans to achieve precise detection and efficient transformation. Due to the high applied value, numerous materials and constructions are adopted for photoelectric effect to deliver on its potential performance. Among these functional materials, metal-semiconductor (MS) or metal-oxide-semiconductor (MOS) systems own unparalleled advantage including reliable stability, superb physical performance, and simple fabrication process. Herein, two types of photoelectric effect, lateral photovoltaic and photo-induced resistance effect, in nanostructure MS or MOS systems are reviewed. These effects have great potential in applications and will play a beneficial role in future investigations. In addition, how each component of the system contributes to the photoelectric properties and responds to external fields are detailed, suggesting future study directions in photoelectric fields.

1. Introduction

Photoelectric effect has long been a central issue in the modern industry and scientific research field since discovered by Heinrich Hertz and explained by Albert Einstein. Due to the special mechanism of interaction between photonics and electrons, the photoelectric effect greatly meets the scientific, industrial, and civilian demands of human beings along with social progress. It is widely used in areas such as microelectronics, detection, solar cells, biophysics, and physical chemistry,[1–7] where research focuses have been dispersed to numerous aspects including higher transformation efficiency, a faster response time, a bigger amplification coefficient, a wider spectral sensitivity, and so forth. In order to achieve the best photoelectric performance in certain conditions, various kinds of materials and architectures are produced and investigated in laboratories and factories. Among numerous photoelectric constructions, metal-semiconductor (MS) or metal-oxide-semiconductor (MOS) structures own prominent merits, such as possessing abundant physical characteristics and cost-efficient fabrication process. Thus, lots of useful devices, especially in photoelectric area, are strongly correlated with MS or MOS structure.[8–15] Over a period of several decades, researches of traditional photoelectric effect have mainly dealt with photoconductivity or photovoltaic effect.[16–19] Photoconductive effect means when under light irradiation, an obvious raising of the material's electrical conductivity occurs, which is caused by the increasing number of free carriers. On the macroscopic perspective, when a bias voltage and a load resistor are used in series with the device, a voltage drop across the load resistors can be measured when the change in electrical conductivity of the material varies the current through the circuit.[20,21] Classic examples of photoconductive effect include photoresistor and photodiode.[22,23] Another phenomenon, photovoltaic effect, is more closely related to the photoelectric effect which utilizes the absorption of photo energy. It includes a proven and prominent technique of solar cells, which is an electrical device that mainly converts solar energy into electricity. Nowadays, relevant technologies of these effects are exploited in industrial systems and admittedly, MS or MOS structures have done well in such areas.[24–30] However, with the technological advancement, especially the development of nanoengineering provides optoelectronics numerous emerging materials and constructions, highly fueling the technological innovation and progress of photoelectric field.[31–36] Here, this feature article presents a review focusing on two typical photoelectric effects, lateral photovoltaic effect (LPE) and photo-induced resistance effect, in nanostructure MS or MOS systems. LPE is a hot issue in areas of photodetection and position sensors, while photo-induced resistance effect is acknowledged to have promising prospects in industrial applications. Both effects take an active part in scientific exploring and benefit a lot from nanotechnology advancements. Specially, a detailed introduction about the

A. H. Dong, Prof. H. Wang
State Key Laboratory of Advanced Optical Communication Systems and Networks
School of Physics and Astronomy
Shanghai Jiao Tong University
800 Dongchuan Road, Shanghai 200240, China
E-mail: huiwang@sjtu.edu.cn
A. H. Dong, Prof. H. Wang
Key Laboratory for Thin Film and Microfabrication of the Ministry of Education
School of Electronic Information and Electrical Engineering
Shanghai Jiao Tong University
800 Dongchuan Road, Shanghai 200240, China

The ORCID identification number(s) for the author(s) of this article can be found under https://doi.org/10.1002/andp.201800440

DOI: 10.1002/andp.201800440

contribution brought by nanoscale materials is exhibited in the following, which is expected to be beneficial for the research in photoelectric fields.

2. Lateral Photovoltaic Effect

The LPE is generally acknowledged as an attribute characteristic of some semiconductor materials since being discovered by Schottky and expanded upon by Wallmark in floating Ge p-n junctions.[37] Hitherto, LPE gets widely used in photoelectric detection and is considered as an effective method to measure the characteristics of materials.[38–40] A deeper understanding of hot functional materials, including transition metal dichalcogenides (TMDCs), carbon isotope, III-V compound semiconductor, MS, and graphene,[41–47] could be learned from experiments of LPE. Moreover, even the surface states of a doped semiconductor can induce a conspicuous LPE.[48,49] Here, we present a review of LPE in the MS or MOS nanostructures. In certain conditions, LPE displays some attractive features due to its strong correlation with the surface or interface of materials.[50–52] Usually, a metallic film of nanoscale deposited on a semiconductor will induce effects different from it in bulk materials, such as localized surface plasmon resonances.[53,54] These effects are mutually reinforced with LPE and promote the photoelectric performance.[55–58]

2.1. Mechanism of LPE in MS or MOS Structure

Along with the progress of science, the theories of LPE have been gradually established. Here, this section presents a carrier diffusion model in the MOS system, which gets widely used in scientific research.[59–63] When a laser with power p irradiates on the metal side between electrode A and B, large quantities of electron-hole pairs are generated in the semiconductor. From the view of electrons, the excited electrons at light point will have chance (possibility of P) to transmit to the metal side due to the nonequilibrium state. Here, the number of excited electrons is defined as n_0 and the number of electrons transmitting to the metal side is defined as N_0, where $N_0 = n_0[1 - P^{\tau p/n_0}]$ and τ is a time-related coefficient. Then, the photo induced excess electrons generate a density gradient in the metal film, resulting in a lateral diffusion away from the irradiation point. Next, these electrons will also have a chance to transmit to semiconductor side in the region without light irradiation and then return to beginning point (as shown in **Figure 1**c). In addition, it can also be explained from the view of electron-hole pairs, as shown in Figure 1d, the electrons and holes diffuse laterally in the metal and semiconductor side under the action of density gradient. Then, these carriers will recombine in the region without light irradiation. Thus, with electrodes on the metal film, an obvious voltage output called lateral photovoltage (LPV) could be observed as shown in Figure 1a.

According to the diffusion equation $D_m \frac{d^2 N(r)}{dr^2} = \frac{N(r)}{\tau_m}$, the electron density at position r in the metal can be written as[62]

$$N(r) = N_0 \exp\left(-\frac{|x-r|}{\lambda_m}\right) \tag{1}$$

Anhua Dong received his B.Sc. in physics from Wuhan University in 2015. He is currently a Ph.D. candidate in Shanghai Jiao Tong University under the guidance of Professor Hui Wang. His current interests mainly focus on the exploration or investigation of new photoelectric effects in nanosized metal-semiconductor structures.

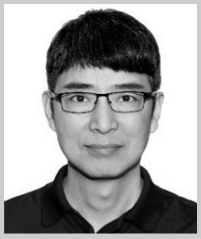

Hui Wang received his Ph.D. from Fudan University and finished his postdoctoral research in Francis Bitter Magnet Lab of MIT. He is currently a professor and research scientist in Shanghai Jiao Tong University. His current interests mainly focus on the exploration or investigation of new photoelectric effects in nanosized metal-semiconductor structures.

Where $D_m = \frac{k_B T}{e^2 \rho N_{F0}}$ is the diffusion constant of metal, $N_{F0} = \frac{8\pi}{3}\left(\frac{2m_e E_{F0}}{h^2}\right)^{\frac{3}{2}}$ is the electron density below Fermi level (E_{F0}), ρ is the metal resistivity, x is the position of the laser point, $\lambda_m = \sqrt{D_m \tau_m}$ is the diffusion length and τ_m is the life time of the diffusion electrons in the metal. Similarly, the electron density at position r in the semiconductor can be written as

$$n(r) = n_0 \exp\left(-\frac{|x-r|}{\lambda_s}\right) \tag{2}$$

When irradiated with a laser, the energy band diagram of the structure is given in Figure 1b. The Fermi levels of metal and semiconductor after illumination at position r can be presented as[62]

$$E_{Fm}(r) = E_{F0} + \frac{1}{4\pi}\left(\frac{\hbar^2}{2m_e}\right)^{\frac{3}{2}} {E_{F0}}^{-\frac{1}{2}} N(r) \tag{3}$$

$$E_{Fs}(r) = E_{F0} + \frac{k_B T}{n_T} n(r) \tag{4}$$

Where $n_T = \frac{2(2\pi m_e k_B T)^{\frac{3}{2}}}{h^3} \exp(-\frac{E_c - E_{F0}}{k_B T})$ is the electron density in semiconductor conduction band.

It is easy to understand that inequable distance between light point and two electrodes will cause different electron density and different Fermi level at two electrodes, thus inducing the LPV. Based on previous calculations, the LPV in the metal and semiconductor side are respectively written as[62]

$$LPV_m \equiv V_{AB} = \frac{E_{Fm}(L) - E_{Fm}(-L)}{e} = K_m N_0 \left[\exp\left(-\frac{|L-x|}{\lambda_m}\right) - \exp\left(-\frac{L+x}{\lambda_m}\right)\right] \tag{5}$$

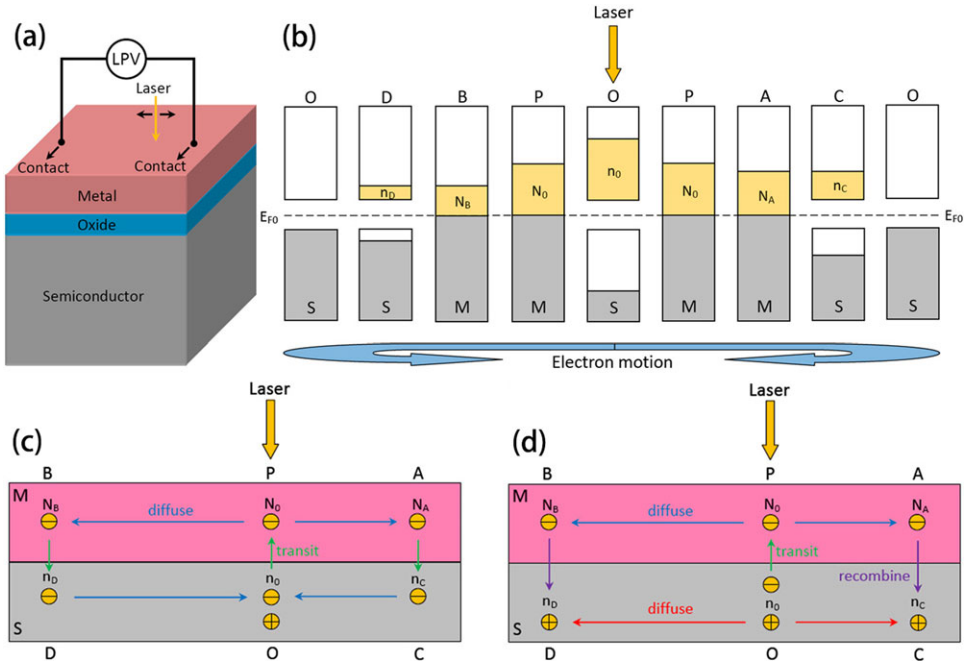

Figure 1. a) Diagram of LPE in a MOS structure. b) The energy band of this structure under laser irradiation. The gray part represents the original equilibrium electrons and the yellow part is the laser-induced nonequilibrium electrons. c) Diagram of pure electron diffusion and d) electron-hole pairs diffusion in the structure. Reproduced with permission.[62] Copyright 2019, Multidisciplinary Digital Publishing Institute.

$$LPV_s \equiv V_{CD} = \frac{E_{Fs}(L) - E_{Fs}(-L)}{e} = K_s n_0 \left[\exp\left(-\frac{|L-x|}{\lambda_s}\right) - \exp\left(-\frac{L+x}{\lambda_s}\right)\right] \quad (6)$$

Where L and $-L$ are the positions of the two electrodes, $K_m = \frac{1}{4\pi e}\left(\frac{\hbar^2}{2m_e}\right)^{\frac{3}{2}} E_{F0}{}^{-\frac{1}{2}}$ is coefficient in the metal side, $K_s = \frac{k_B T}{e n_T}$ is coefficient in the semiconductor side. If $L = \lambda_m(\lambda_s)$, the LPV can be idealized as

$$LPV_m' = \frac{2K_m N_0}{\lambda_m} \exp\left(-\frac{L}{\lambda_m}\right) x \quad (7)$$

$$LPV_s' = \frac{2K_s n_0}{\lambda_s} \exp\left(-\frac{L}{\lambda_s}\right) x \quad (8)$$

This diffusion model clearly shows the relation between LPV and structural characteristics. Moreover, it can also apply to p-n junction, semiconductor heterojunction, and Schottky junction. However, there still exist some exceptions where the LPE is considerably influenced by the Dember effect or thermal effect,[64] which would not be discussed here. Besides, other theoretical models about LPE are reported by Lucovsky, Levine et al., and Niu et al.[65–67] which are applicable as well in certain conditions. Utilizing these results, numerous materials and constructions are employed to provide advantages in applications such as photodetections and photoelectric sensors, which will be introduced as follows.

2.2. LPE Contributed by Different Materials and Constructions

2.2.1. Contributions Made by Nanosized Metal Films

Metal materials are very crucial in the MS systems. Liu and Yu et al. have reported the effect brought by metal on the photoelectric performance of MS systems.[68,69] **Figure 2** shows the experimental results in the structures of $Cr/SiO_2/Si$ and Co/Si, where the Co/Si structure will be discussed minutely. Derived frombrk Figure 2, the spectrum has quite diverse responses to the systems with different structures and materials. Thus, to reveal the relation between light sensitivity k and other parameters, a series of calculations have been done through combining the diffusion model and band theories. Hence, sensitivity k can be presented as[68]

$$k(\lambda, d) = \frac{2K_1 K_2 (h\lambda/c - E_g)^{\alpha-\beta}}{K_3(d-d_0)} \times \exp\left[-\frac{L}{K_3(d-d_0)(h\lambda/c - E_g)}\right] \quad (9)$$

Where K_1, K_2, K_3, and α, β, τ are different coefficients, d and d_0 respectively represent metal thickness and threshold thickness, λ represents laser wavelength, E_g is the energy gap of the semiconductor and L is half of the distance between the electrodes.

Equation (9) is consistent with the experimental results shown in Figure 2 and gives a comprehensive description of the correlation among sensitivity, wavelength, and metal thickness. As discussed in the mechanism section, LPE of metal has a great bearing on the diffusion length, which has a disparity for various materials and is greatly influenced by the metal thickness. Thus,

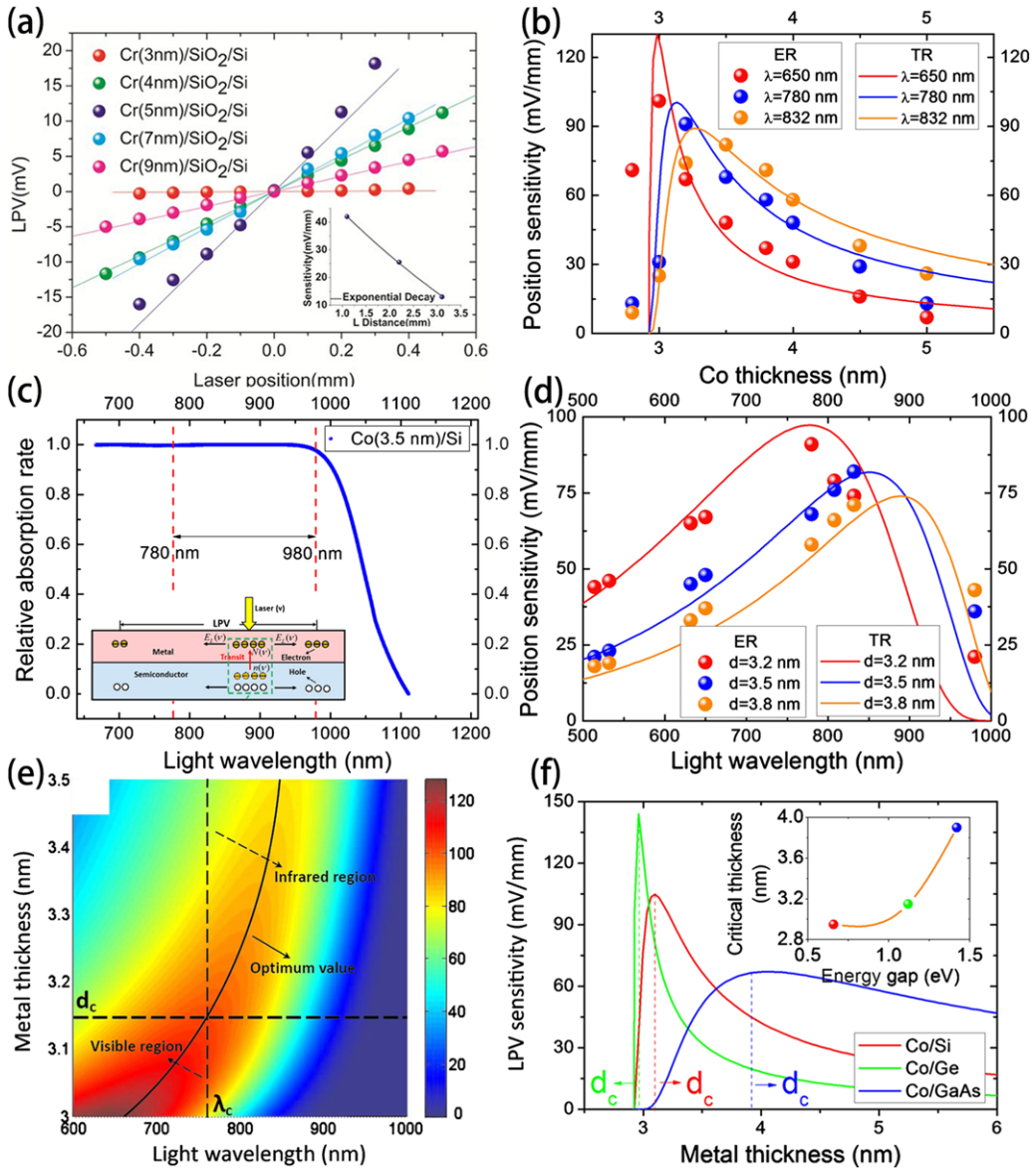

Figure 2. a) LPV as a function of laser position in the structure of Cr/SiO_2(1.2 nm)/Si with different Cr thickness under laser irradiation of 5 mW and 635 nm. b) Position sensitivity of different wavelength in the structure of Co/Si as a function of Co thickness. c) Normalized absorption rate of infrared region in the structure of Co/Si. d) Position sensitivity as a function of wavelength with different Co thickness in the structure of Co/Si. e) LPV sensitivity as a function of both wavelength and Co thickness in the structure of Co/Si. f) LPV sensitivity as a function of Co thickness in different structures of Co/Si, Co/Ge, Co/GaAs. Where experimental results (theoretical results) are written as ER (TR). λ_c (d_c) means a critical wavelength (thickness) distinguishing the visible and infrared regions. The parameters are Eg(Si) = 1.12 eV, Eg(Ge) = 0.66 eV, Eg(GaAs) = 1.42 eV, λ = 760 nm, d_0 = 2.9 nm, α = 0.5, β = 2. Reproduced with permission.[68] Copyright 2019, American Institute of Physics. Reproduced with permission.[69] Copyright 2019, Optical Society of America.

an appropriate metal thickness is crucial to the photoelectric performance for diverse structures and spectrum. This statement is proven in experiments shown in Figure 2a,b. In the certain structure of Cr/SiO_2(1.2 nm)/Si, the optimum Cr thickness of LPE is 5 nm. While in the structure of Co/Si, the optimum Co thickness of LPE for laser wavelength of 650, 780, and 832 nm is respectively 3, 3.2, and 3.5 nm. In addition, Figure 2e shows the LPV sensitivity as a function of both wavelength and metal thickness. Clearly, there exists an optimum combination of wavelength and metal thickness to obtain the best photoelectric performance. It can also be seen from Figure 2f that LPE performs diversely on different semiconductor substrates. As mentioned above, different metal films and thickness induce diverse spectral response and sensitivity, demonstrating the importance of the categories and configurations of metal materials on the photoelectric performance of MS or MOS systems.[70–73]

Moreover, recently developed 2D materials have been employed to combine with semiconductors. As is known, photodetection devices using 2D materials usually exhibit a fast response time and high sensitivity.[41,74–78] Similar to the metal films,

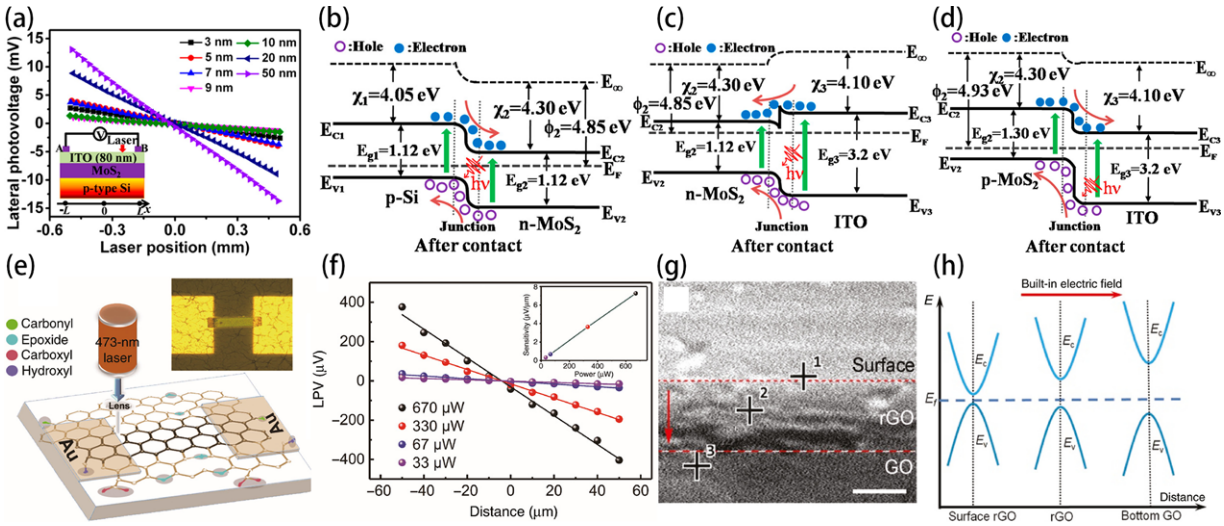

Figure 3. a) LPV as a function of laser position with different MoS_2 thickness. Inset is the diagram of ITO(80 nm)/MoS_2/p-Si irradiated by laser of 532 nm and 10 mW. b) Schematic of energy band of MoS_2 (n-type)/p-Si heterojunction at equilibrium. c) Schematic of energy band of ITO/MoS_2 (n-type) heterojunction at equilibrium. d) Schematic of energy band of ITO/MoS_2 (p-type) heterojunction at equilibrium. e) Diagram of the laser-scribed rGO/GO/SiO_2/Si structure. Laser scribing is carried out using a laser of 473 nm and 580 mW. Brown hexagons represents GO (thickness of 1 μm) and black strap (100 $\times$ 30 μm^2) between Au electrodes represents rGO. Colored circles mean different oxygen-containing groups. The distance between Au electrodes is 100 μm. Inset is a photograph in top view of the real sample. f) LPV as a function of laser position with different laser power and inset is the sensitivity at varied laser power. g) Inclined cross-sectional SEM image of a thick rGO/GO structure, whose scale bar is 1 μm. h) Diagram of the energy alignment across the rGO film. Reproduced with permission.[74] Copyright 2019, American Chemical Society. Reproduced with permission.[75] Copyright 2019, Walter De Gruyter.

thickness of 2D material deposited on semiconductor substrate is also a crucial factor affecting the photoelectric performance of devices. Qiao et al. has reported an abnormal thickness dependent LPE in ITO/MoS_2/p-Si structure.[74] Generally, LPE in MS structures own a uniform variation tendency that as the thickness of metallic film increases, the output of LPV will rise dramatically in the beginning and then decrease gradually. However, the LPV in ITO/MoS_2/p-Si structure is quite inconsistent with it. As shown in **Figure 3**a, the increment rate of LPV grows from 5.31 to 8.44 mV mm^{-1} as the MoS_2 thickness increases from 3 to 5 nm. But it decreases to a minimum of 2.47 mV mm^{-1} as the MoS_2 thickness reaches 9 nm. Then, the rate rises significantly to 18.86 and 26.81 mV mm^{-1} as the MoS_2 thickness reaches 20 and 50 nm. Finally, when the MoS_2 thickness is larger than 50 nm, the LPV gradually decreases (not exhibited in the figure).[74] This abnormal variation is mainly ascribed to the reversal of built-in field at ITO/MoS_2 interface induced by the n to p-type transformation of MoS_2. At first stage (MoS_2 thickness is 3 nm), the barrier at MoS_2/p-Si (B_1) and at ITO/MoS_2 (B_2) are respectively shown in Figure 3b,c, where MoS_2 is n-type and electrons would diffuse into MoS_2 from p-Si and ITO. In this situation, built-in field caused by B_1 is much larger than caused by B_2. When the thickness increases to 5 nm, the height of B_1 rises and of B_2 decreases (reverse enhanced), inducing a larger LPV. Then, as the thickness rises from 5 to 10 nm, both the height of B_1 and B_2 decreases, resulting in the decline of LPV. However, if the thickness continues to grow (to 50 nm), the height of B_1 still decreases but B_2 improves greatly (forward enhanced). The MoS_2 changes from n to p-type (shown in Figure 3d) and accelerates the electrons' separation and transmitting from Si to ITO, which is responsible for the dramatic enhancement of LPV. Detailed explanation and verification are presented in the reference. The results show that the performance of 2D materials can be modulated by thickness.

Besides, 2D materials own some intrinsic factors affecting the photoelectric performance. Feng et al. has reported a conspicuous LPE in reduced graphene oxide (rGO)/graphene oxide (GO)/SiO_2/Si structure.[75] In contrast to the common methods of thermal or chemical reduction, the reduction of rGO is controlled by laser scribing. The schematic of the device is shown in Figure 3e, where the brown hexagons are GO films obtained by drop casting on SiO_2/Si wafer. Without reduction, GO films always contain series of oxygen-containing groups (colored circles). In this experiment, a laser of 473 nm and 580 mW is employed to sweep between Au electrodes at a constant rate. After the laser reduction, part of the oxygen-containing groups is removed and a black strip of rGO is formed, which bridges the two Au electrodes. Figure 3f shows the experimental results of LPV measured in this laser-scribed structure with different laser power, where the LPV gets larger as the laser power increases. Particularly, this LPV is much larger than it measured in thermal rGO device with the same construction. In addition, the maximal nonlinearity is 5.4% and the measured response time is 1.6 ms (rise) and 1.9 ms (decay), both of which are very prominent in rGO-based devices.[75] These properties can be attributed to a gradient junction across the rGO films. Due to the optical filter effect of the upper rGO layer and finite penetration length of the laser, reduction degree of rGO layers at different depth is distinguishing, which is responsible for the formation of gradient junction across the rGO film. The gradient junction leads to a built-in electric field pointing to the bottom that accelerates the generation and separation of photo induced carriers, and finally causes a large LPV. The existence of gradient junction can be verified through the

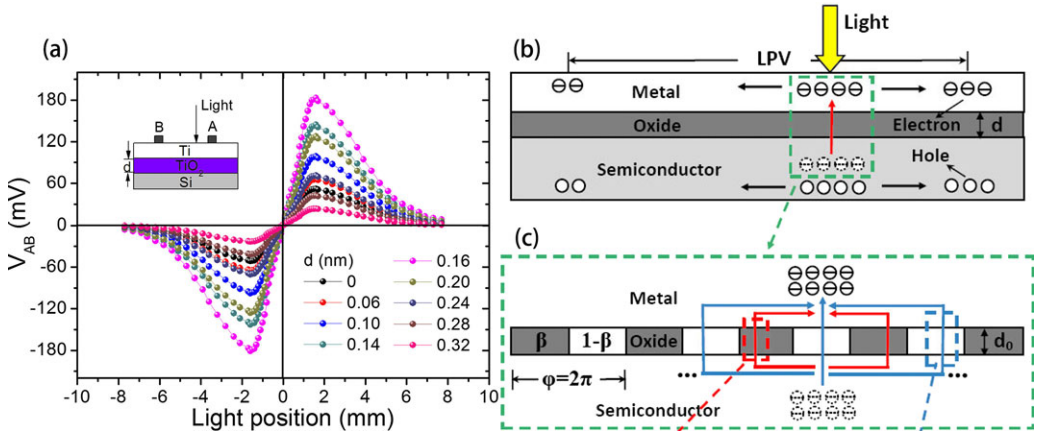

Figure 4. a) LPV (V_{AB}) as a function of laser position in Ti/TiO_2/Si structure with different oxide thickness (color lines). Inset is the device schematic. b) Mechanism of LPE in the structure with a fully covered oxide layer. c) Mechanism of electronic interference in the structure with un-fully covered oxide layer when excited electrons transmit from semiconductor to metal. The red (blue) arrows represent the electrons tunneling through the walls (passing through the windows). Reproduced with permission.[61] Copyright 2019, American Institute of Physics.

scanning electron microscope (SEM) images and energy alignment shown in Figure 3g,h. The carbon/oxide (C/O) ratio of points 1–3 in the SEM image can be determined by energy-dispersive spectroscopy (EDX). As expected, the ratio decreases, as the position gets deeper. Combined with the energy alignment, the formation of gradient junction is proven and so does the existence of built-in field. If the rGO layer is produced through thermal method, the reduction degree is uniform and there does not exist a significant gradient junction, which is responsible for the decrease of LPV. Above statements show that the configuration of 2D materials can not only change the experimental performance but even induce a variation of material properties. Compared to the metal materials, this unique effect is expected to play an active role in the emerging devices.

2.2.2. Contributions Made by Nanosized Oxide Layers

Mentioned works have dealt with the nanosized metal materials, yet there also exist some oxide constructions with commendable functionality adopted in LPE. Generally, oxide layers are considered to deteriorate the LPV due to the decrease of electron tunneling possibility from semiconductor to metal. However, Yu et al. reports an opposite results by inserting an TiO_2 layer in Ti/Si structure.[61] These LPV experimental results are displayed in **Figure 4**a, where LPV with TiO_2 thickness of 0.16 nm (purple line) reaches the maximum and with thickness of 0.32 nm (pink line) reaches the minimum (lower than it in Ti/Si structure without oxide layers). The key point here is whether the oxide layer could fully cover the semiconductor substrate. As previously investigated, a monolayer TiO_2 (001) has a thickness about 0.30 nm (defined as d_0).[79] When the thickness of TiO_2 layer is smaller than 0.30 nm, it will not own enough molecules to fully cover the semiconductor substrate and results in the formation of discrete islands of TiO_2, whose schematic is shown in Figure 4c. The empty part is called "window" and the covered part is called "wall", where a proper ratio of d/d_0 represents a periodical array of the windows and walls. When electrons transmit from semiconductor to metal forced by the built-in electric field near the light position, they can either pass through the windows or tunnel through the walls. Therefore, the wave function of transiting electrons could be written as[61]

$$\psi = \sum_{1-\beta}\phi(r) + \sum_{\beta}\phi(r)e^{-d_0/d_t}(0 < d < d_0); \psi$$

$$= \int_r \phi(r)e^{-d/d_t}dr(d \geq d_0) \quad (10)$$

Where d and d_t represents the thickness of the TiO_2 layer and electron tunneling length in the oxide layer, $\beta = d/d_0$ is the ratio, meaning there will be β% of the region covered by oxide molecules (wall) and (1-β)% is empty (window).

Like a light goes through a Fresnel zone plate, the subwave function with positive phase can directly pass through the windows, while the one with negative phase will be obstructed by the walls. This results in the enhancement of electron interference and LPV. Then, as the thickness of oxide layer increases and the substrate is fully covered, electron transition from semiconductor to metal becomes more difficulty and induces a decline of LPV. That is to say, the oxide thickness has a major impact on the performance of MOS systems.

It has been learned that a discrete TiO_2 layer can affect the photoelectric characteristic. Moreover, Hao et al. has demonstrated that a consecutive (fully covered) oxide layer can also play a significant role in photoelectric performance in $MoS_2/SiO_2/Si$ structure,[42] where MoS_2 film is deposited by magnetron sputtering technique. **Figure 5**a shows the LPV experimental results in $MoS_2/SiO_2/Si$ and MoS_2/Si structures. In comparison of MoS2/Si structure, $MoS_2/SiO_2/Si$ structure owns a larger LPV, meanwhile it also shows a superb linearity with laser position. It is necessary to learn the reason of variation after the incorporation of SiO_2 layer. As is known, the mechanism of LPE in this device is similar with that mentioned above. That is, under laser illumination, the electron-hole pairs are excited and separated by the built-in electric field in the heterojunction, then diffuse laterally to electrodes and cause the LPV as shown in Figure 5b.

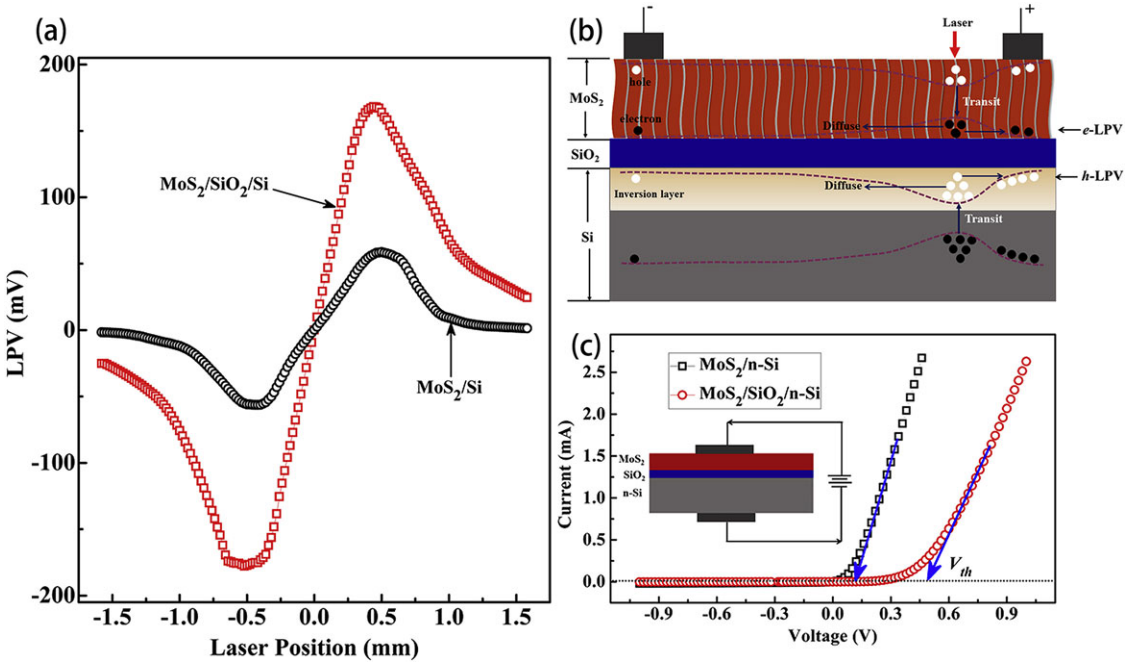

Figure 5. a) LPV as a function of laser position in $MoS_2/SiO_2/Si$ and MoS_2/Si structure. The distance between electrodes is 1.0 mm, the thickness of MoS_2 and SiO_2 are respectively 60 nm and 3 nm b) Schematic of the measurement and mechanism of LPE in $MoS_2/SiO_2/Si$ structure. c) Longitudinal I–V curve of this device with and without SiO_2 layer (3 nm). Reproduced with permission.[42] Copyright 2019, Elsevier.

Here, in this case, the enlargement of built-in electric field is one of the main reasons for this feature. As proven in the experiment shown in Figure 5c, a longitudinal I–V curve of this device is measured with and without SiO_2 layer of 3 nm. The threshold voltage (V_{th}) is 0.11 V of MoS_2/Si and 0.49 V of $MoS_2/SiO_2/Si$, which is determined by the built-in electric field at the interface.[80] The larger threshold voltage demonstrates that there exists a stronger built-in field in $MoS_2/SiO_2/Si$ structure, then inducing a larger quantity of excited carriers and resulting in the higher LPV.

Another reason for this feature is the variation of interface conditions after the incorporation of the SiO_2 layer. Compared with bare Si substrates, SiO_2/Si substrates can supply much smoother surface for crystal growth, which brings a higher uniformity at the interface. This variation of interface will result in a change of the growth pattern of MoS_2, which has been reported to impact greatly on the photoelectric properties.[81,82] Usually, (001) plane of MoS_2 is a stable state and parallel to the substrate surface, while (100) plane is a metastable state and perpendicular to the substrate surface.[81] However, it is worth mentioning that such kind of vertically oriented MoS_2 has been proven to own a better photoelectric performance by Cong et al. (as shown in **Figure 6**a,b).[82] Here follows the discussion of $MoS_2/SiO_2/Si$ structure, Figure 6c shows the cross-section views of SEM images of MoS_2 films, which is deposited by magnetron sputtering technique with thickness of 350 nm grown on the Si substrate. Distinctly, the MoS_2 films consist of large quantities of nanosheets which stand vertically to the interface (MoS_2(100)). However, at the SiO_2(3 nm)/Si substrate, a different growth mode can be seen clearly as shown in Figure 6d. In a range of thickness up to 5 nm, the atomic layer of MoS_2 is horizontally lying on the substrate (MoS_2(001)) and it is converted to be perpendicular to the substrate (MoS_2(100)) as the MoS_2 thickness increases. This is mainly because at the beginning (thickness <5 nm), the atoms of Mo and S can move freely on the substrate with a high diffusion rate due to the smooth surface supplied by SiO_2 passivation layer. In this case, the stable state (MoS_2(001)) predominates the growth of MoS_2 film and the atomic layers are horizontally lying on the substrate surface. However, as the MoS_2 thickness increases (thickness >5 nm), the surface becomes rough and the diffusion rate decreases, which causes the following vertically standing layer. In this special construction, the horizontal MoS_2 layer can form high quality interface with few trap states and the vertical one can facilitate carrier transmitting from the interface to top layer. These results exhibit several advantages benefited from the incorporation of oxide layers, expanding the range of applications and functionality of oxide materials.

2.2.3. Contributions Made by Surface Morphologies of Semiconductors

Besides the metal or oxide materials in nanoscale, nanostructure semiconductor materials can also bring remarkable benefits to the properties of LPE. Mei et al. have demonstrated a huge enhancement of photoelectric performance in silicon-nanowire-modified Ag/Si structure,[83] where the silicon nanowires (SiNWs) were fabricated by metal-assisted chemical etching (MACE).[84–86] **Figure 7**a–c shows the surface morphologies (Top view of SEM images) of SiNWs, SiNWs with silver nanoparticles, and Silver nanoparticles on Si substrate. The corresponding experimental results of LPV are shown in Figure 7e. Compared to Ag/Si samples, the LPV of Ag/SiNWs/Si structures get a considerable increase, whose maximum sensitivity reaches 65.35 $mV \cdot mm^{-1}$ (50 times larger than it in Ag/Si). The main

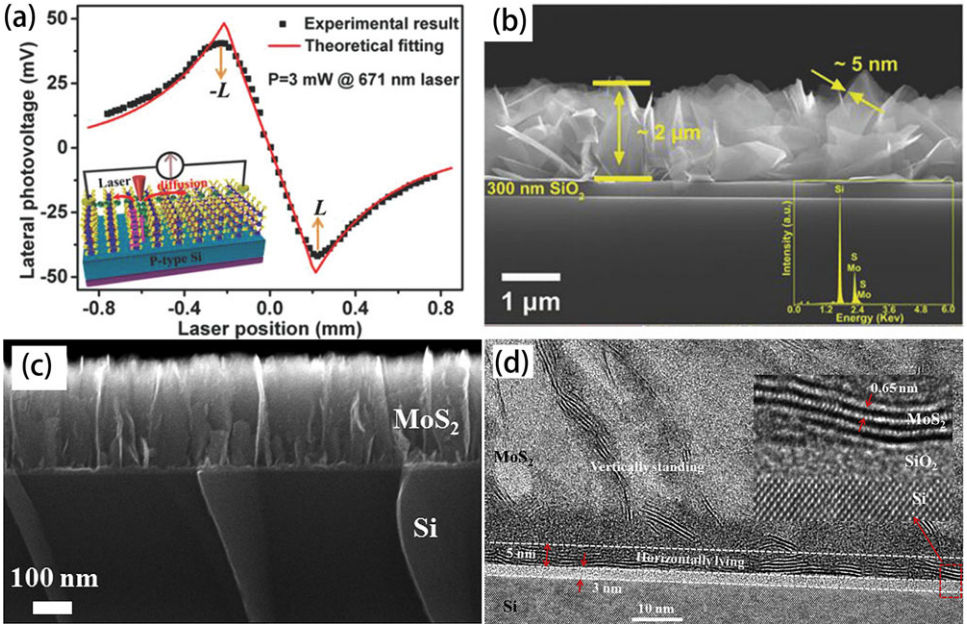

Figure 6. a) LPV as a function of laser position. b) cross-section views of SEM images of vertically oriented MoS_2. c) Cross-section views of SEM images of 350 nm MoS_2 films on the Si substrate. d) Cross-section view of high-resolution transmission electron microscope (HRTEM) images of the $MoS_2/SiO_2/Si$ structure. Inset displays an enlarged HRTEM image near the interface. (a) and (b) are in the structure in ref. [82]. Reproduced with permission.[82] Copyright 2019, Wiley-Blackwell. (c) and (d) are in the structure in ref. [42]. Reproduced with permission.[42] Copyright 2019, Elsevier.

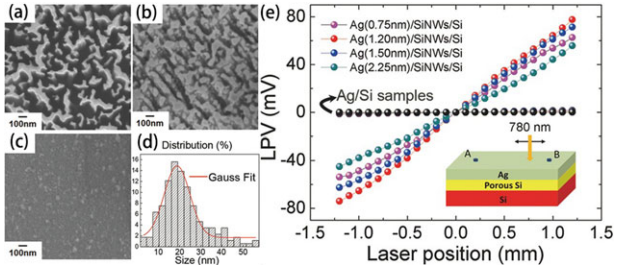

Figure 7. Top view of SEM images of a) SiNWs, b) SiNWs with silver nanoparticles, c) Silver nanoparticles on Si (n-type) substrate, d) Size distribution of silver nanoparticles on SiNWs. The silicon substrates are n-type (111) Si wafers of 0.3 mm and 50–80 Ω cm at room temperature. e) LPV as a function of laser position in Ag/SiNWs/Si structures with different thicknesses of silver film. The insets are the measurement schematic, where the distance between two electrodes is 2.5 mm and the origin point is set in the middle between A and B. The laser is of 780 nm and 145 mW. Reproduced with permission.[83] Copyright 2019, Wiley-Blackwell.

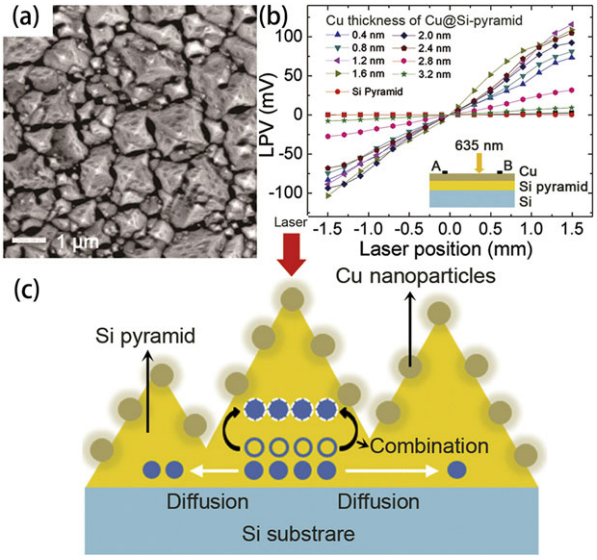

Figure 8. a) Top view of SEM images of Cu(1.6 nm)/Si-pyramid structure. b) LPV as a function of laser position with different Cu nominal thickness. The distance between the two electrodes is 3.0 mm. The origin point is set in the middle between A and B. c) Mechanism schematic of LPE in Cu/Si-pyramid structure. Reproduced with permission.[89] Copyright 2019, Institute of Physics Publishing.

reason for this feature is that SiNW structure has a higher absorption and lower reflection of light, which leads to light harvesting in the system and produces more electron-hole pairs.[87,88] In addition, the ultrathin Ag film in SiNWs structure raises the sheet resistance of the system, which is also responsible for the increase of LPV according to the theories.

A similar construction of copper-nanoparticle-covered random Si nanopyramids (Cu/Si-pyramid) is also proven to achieve an enhancement of photoelectric performance,[89] indicating a wide applicability of such types of nanostructure. **Figure 8**a shows the top view of SEM images of this structure. When irradiated by laser, the system with suitable thickness presents a conspicuous LPE with a high sensitivity (maximum reaches 157.9 $mV \cdot mm^{-1}$) as shown in Figure 8b. This surface morphologies of random nanopyramids bring a low surface recombination and more optical resonance modes, which cause a greater light harvesting (shown in Figure 8c) and benefit the performance of LPE a lot.[90]

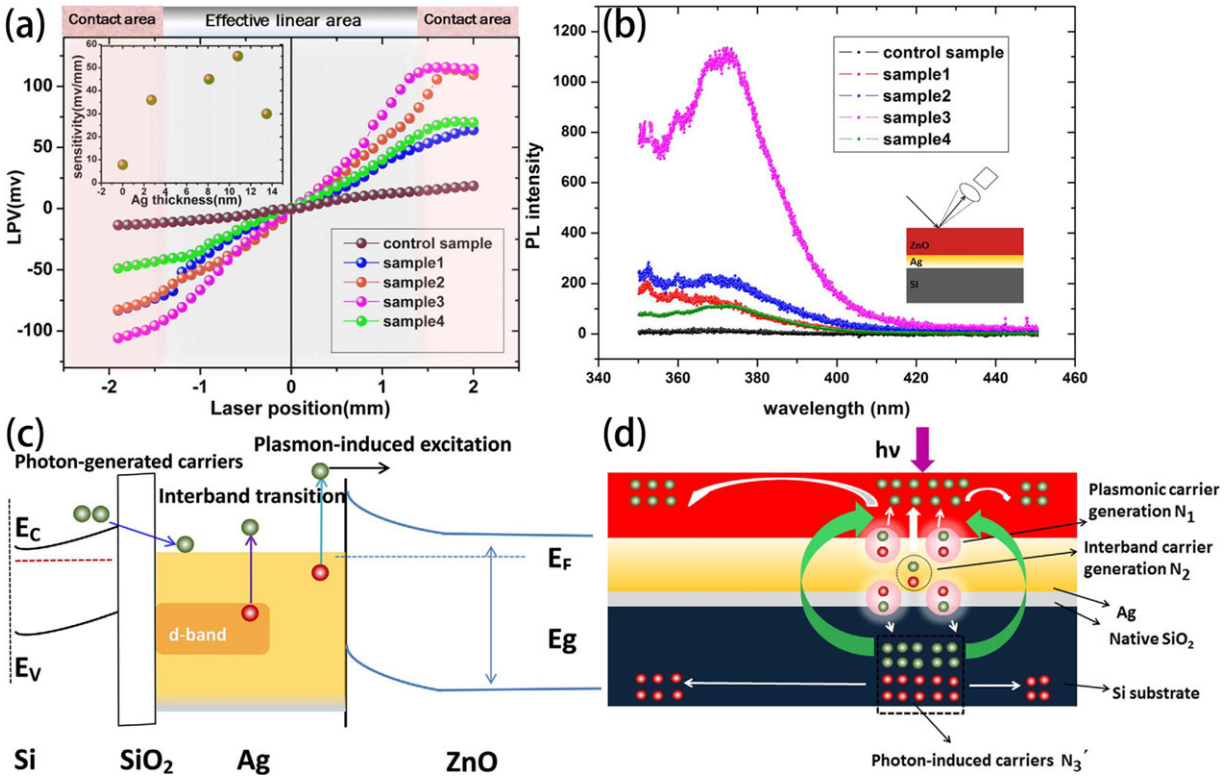

Figure 9. a) LPV as a function of laser position in ZnO/Ag/n-Si (111) structure irradiated by a laser of 405 nm and 4 mW. The Ag thickness of sample 1–4 are 2.7, 8.1, 10.8, and 13.5 nm (0 for control sample). The ZnO thickness is approximately 28.5 nm. b) PL spectra of the silver semicontinuous film mediated ZnO hybrid nanostructures. c) Energy band diagram of the ZnO/Ag/Si structure. d) Mechanism schematic of the LSP induced carrier excitation. Reproduced with permission.[95] Copyright 2019, Springer Nature.

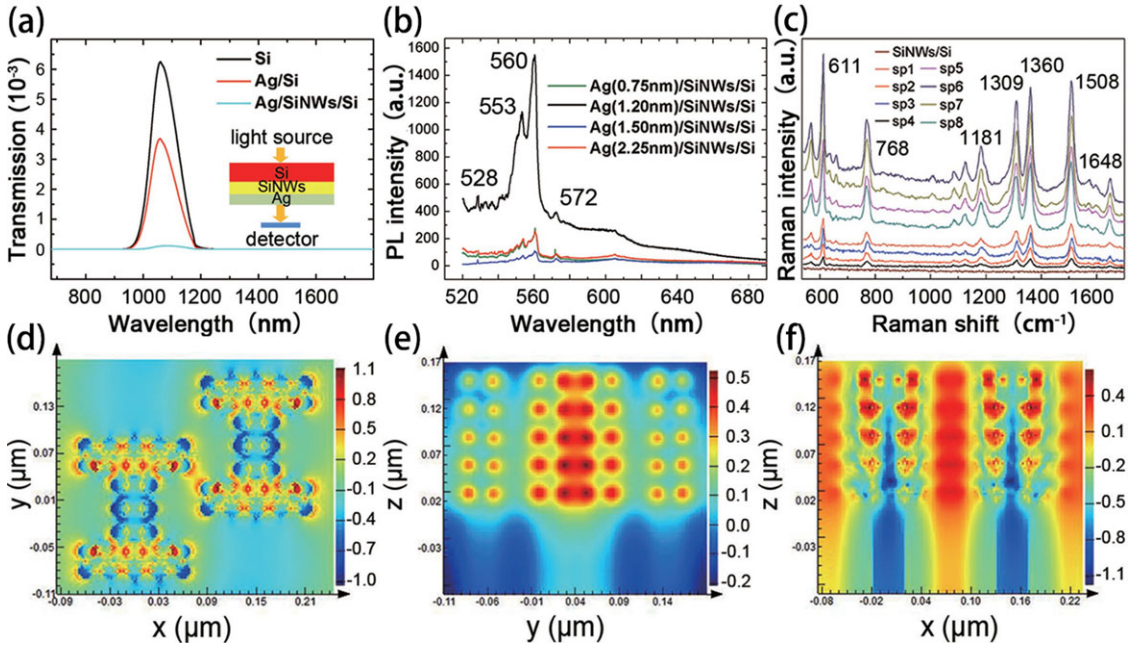

Figure 10. a) NIR spectra of the Si, Ag/Si and Ag/SiNWs/Si structures. Inset displays the measurement schematic. b) PL spectra of the Ag/SiNWs/Si samples with different thickness of silver film. c) surface-enhanced Raman scattering (SERS) spectra of 10^{-8} m Raman spectra of rhodamine-6G (R6G) obtained on three kinds of structures. d) Under laser irradiation, FDTD simulations of Ag/SiNWs/Si structures in x–y, e) y–z, and f) x–z planes. Reproduced with permission.[83] Copyright 2019, Wiley-Blackwell.

The reference also displays a simulation of this system whose result is consistent with above statements as well.

In addition, there exists another typical way of ion doping to alter the interfacial conditions and then enhance the photoelectric properties. Yildirim et al. makes a Al/ZnO/p-Si stratified structure where the ZnO layers are In doped with different concentration.[91] It is noticeable that the surface morphology changes a lot after doping. According to the atomic force microscope (AFM) images of the surficial conditions, the roughness of ZnO interlayers (diameter of fibers) increases with In dopant. Though the In ion decreases rectifying properties due to the large decline of series resistance, the light responsivity increases a lot because of the better light absorption and carrier transportation in doped layer, which provides an additional way to adjust the photoelectric properties.[92,93]

2.3. LPE Contributed by Localized Surface Plasmon Resonances

It has been elaborated that the materials can make an enormous impact on the photoelectric performance of MS or MOS systems. Besides, a specific architecture (such as silver embedded nanoscale metal-dielectric composite materials) can also contribute a lot to photoelectric properties by inducing highly localized surface plasmons (LSPs) from visible to near-infrared (NIR) regions.[94] This phenomenon is a kind of collective electron charge oscillations in certain structures that causes a large enhancement of local electric fields when under light irradiation. A detailed explanation of this effect is given by Zhang et al. as follows.[95] When irradiated with a laser, the device of ZnO/Ag/Si structure with particular Ag thickness shows a remarkable amplification of LPE. **Figure 9**a shows the LPV as a function of laser position measured in ZnO/Ag/n-Si(111) structure with different silver thickness of 2.7 nm (sample 1), 8.1 nm (sample 2), 10.8 nm (sample 3) and 13.5 nm (sample 4). Obviously, sample 3 presents the maximum LPV which is seven times larger than it in the control sample. This result is consistent with the photoluminescence (PL) spectra shown in Figure 9b, where sample 3 owns the strongest PL peak. Here, this unexpected amplification is ascribed to the existence of LSP resonance, which is highly sensitive to the composition of the system. As is proven in the experiments, LSP resonance can enhance the local electric fields and then boost the conduction electron excitation process, along with the plasmonic carrier generation caused by interband and intraband transition.[96–98] Thus, LSPs would trigger three concurrent processes as shown in Figure 9c,d, resulting in a larger amount of photon-induced electrons and enormous increase of LPV.

Such LSP induced photoelectric enhancement is also found in the mentioned SiNWs modified Ag/Si structures.[83] Likewise, in this system, strong LSPs are induced by silver nanostructure modified SiNW arrays. It leads to a more efficient light absorption, which is proven in near-infrared (NIR) spectra in **Figure 10**a, and help with the radiating fluorescence emission. Besides, the PL spectra shown in Figure 10b can demonstrate the existence of dangling bonds, which is strongly correlated with LSPs.[55] These dangling bonds produce amphoteric traps with levels near the conduction and valence bands.[99] Then, the traps will cause a bigger lateral concentration gradient and a stronger electric field in SiNWs, which is responsible for the enhancement of LPV. Figure 10c shows the Raman spectra, where Ag/SiNWs/Si structures cause the strongest Raman signal. Figure 10d–f are the finite-different time-domain (FDTD) simulation of electric field distributions in x-y, y-z, and x-z planes, whose results are highly consistent with the experiments. Therefore, a well-designed architecture can induce a unique effect and promote the performance greatly, which provides a scheme for the boost of photoelectric devices.

2.4. LPE Tuned by External Fields

Facts proved that LPE is considerably susceptible to the materials and constructions. Moreover, in some cases, LPE is also sensitive to the external conditions including magnetic field and voltage bias.[100–102] In particular, the magnetic susceptibility are strongly correlated with the metallic materials adopted in the systems.[103,104] Wang et al. combines soft ferromagnetic (FM) materials with semiconductor (Si) and finds that, both the LPV of the FM and Si layer are coupled to the magnetic alignment of the FM layer.[105] **Figure 11**a shows the diagram of experimental

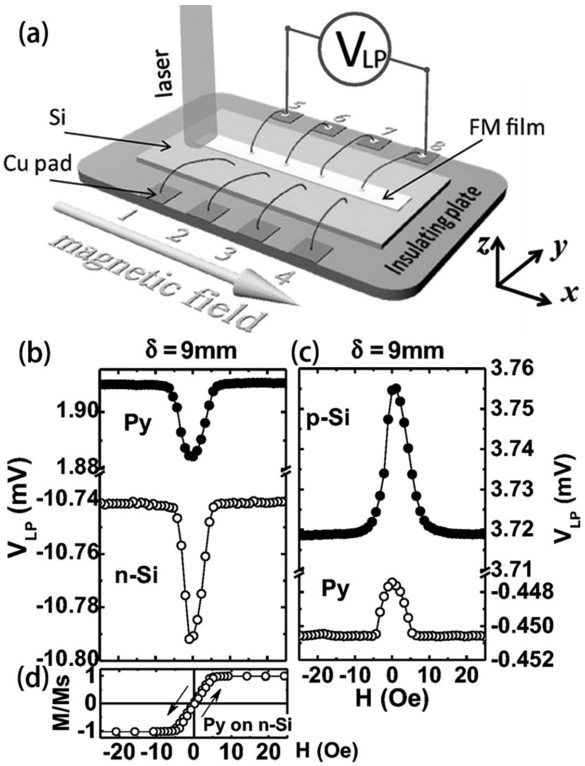

Figure 11. a) Diagram of experimental measurement in the structure of Permalloy(Py)/Si. LPV is measured between electrodes on the FM film. The distance between two electrodes fixes at 9 mm. A magnetic field is applied perpendicular to the easy magnetization (y) axis. The laser irradiates on the point of $x = 0$ and its power is 30 mW. b) LPV (V_{LP}) as a function of magnetic field in the structures of Py/n-Si and c) Py/p-Si. d) Normalized magnetization of the Py layer, measured at room temperature. Reproduced with permission.[105] Copyright 2019, Wiley-Blackwell.

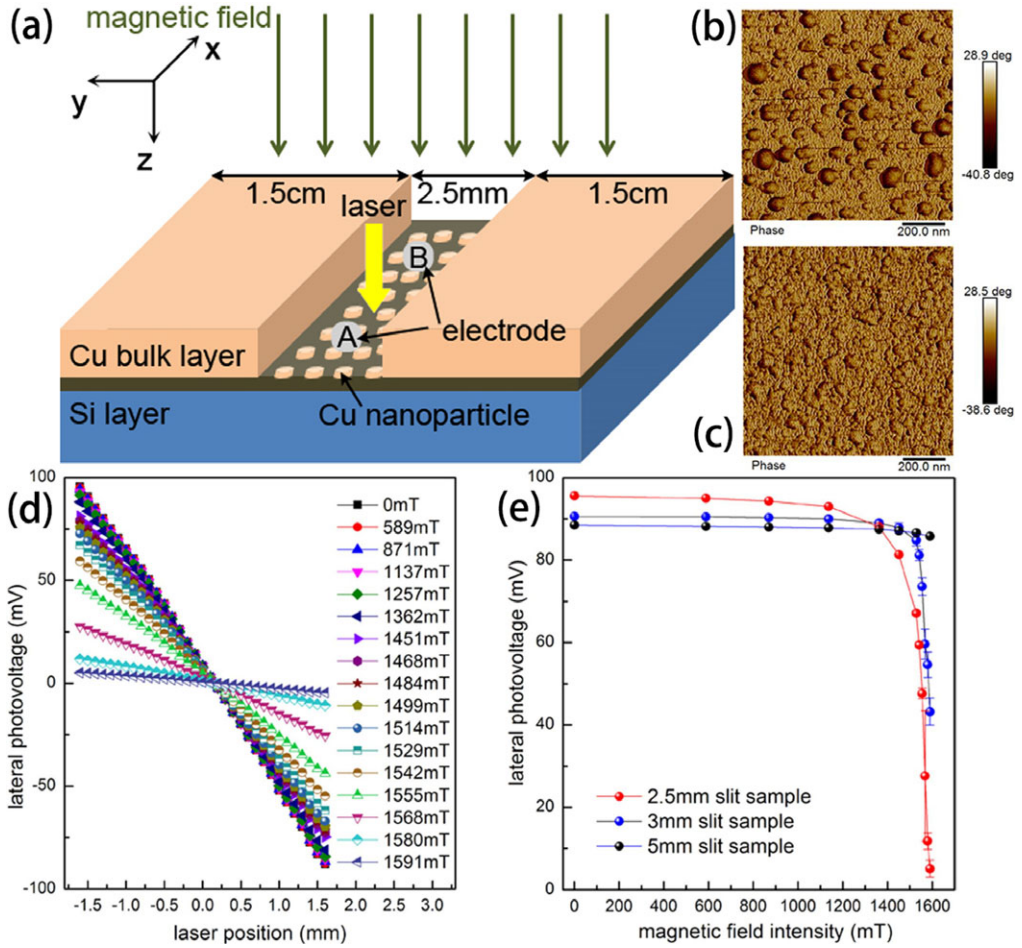

Figure 12. a) Diagram of the designed MOS structure in a magnetic field. b) Top view of AFM images of the slit area (central region), where the average thickness is 2.46 nm. c) Top view of AFM images of the edge areas, where the average thickness is 16.4 nm. d) LPV as a function of laser position with different magnetic fields. e) LPV as a function of magnetic field with different widths of the slit area (the laser point is fixed). Reproduced with permission.[106] Copyright 2019, Springer Nature.

measurement, where Permalloy($Ni_{80}Fe_{20}$) is adopted as the FM material in this structure. The results of LPV (V_{LP}), measured in a magnetic field applied along the hard axis of the FM layer (x-axis), are displayed in Figure 11b,c. It could be clearly learned that both the LPV in structures of Permalloy(Py)/n-Si and Py/p-Si vary rapidly when the magnetic field (H) deviates from the origin. This is mainly attributed to reorientation of the magnetic moment. This statement is proven in Figure 11d that the magnetic moment of the Py layer rotates with the magnetic field at $|H|<5$ Oe and saturates at $|H|>5$ Oe. The reorientation influences the resistivity of the FM layer and the lateral diffusion or drift of the excited carriers. Meanwhile, the nonmagnetic Si becomes magnetically susceptible through coupling to the FM layer, finally inducing the magnetic sensitivity of LPE.

Besides utilizing the FM materials, there exists another way to achieve a magnetically susceptible LPE. Zhou et al. has built a special architecture using nonmagnetic MOS systems of $Cu/SiO_2/n$-Si and optical injection, obtaining a conspicuous magnetic sensitivity as high as 520 mV T^{-1}.[106] **Figure 12**a illustrates the schematic of the designed structure. In the central region, there exists a slit area (thickness of 2.46 nm) where Cu nanoparticles are distributed discontinuously (shown in Figure 12b). Figure 12d displays the LPV in the slit area as a function of laser position with different magnetic fields. It can be learned that the nonmagnetic LPV sensitivity is 57.4 mV mm^{-1}, while under the magnetic field of 1.59 T, the sensitivity decreases to 3.0 mV mm^{-1} and the rate of descent should reach 94.8%. Interestingly, this huge variation does not exist in uniform metal films. The phenomenon exactly belongs to the structures with slit area. A further investigation in such structures with different widths of slit area is given in Figure 12e. Obviously, under magnetic field of 1.3 to 1.6 T, a sharp decreasing slope appears in the samples with widths of 2.5 and 3 mm. Before 1.3 T, the decreasing slope is 5.4 mV T^{-1} but it reaches 520 mV T^{-1} when the magnetic field increases from 1.3 T to 1.6 T. It is mainly ascribed to the channel type construction and the illustration is presented as follows.

Due to the visible distinction between the slit area (with discontinuous Cu nanoparticles) and bulk Cu layers, the Cu film can be described as anisotropic in the central region. At the edges of slit area, a lateral built-in field appears (working as a diode as shown in **Figure 13**a) because the Schottky barrier height of

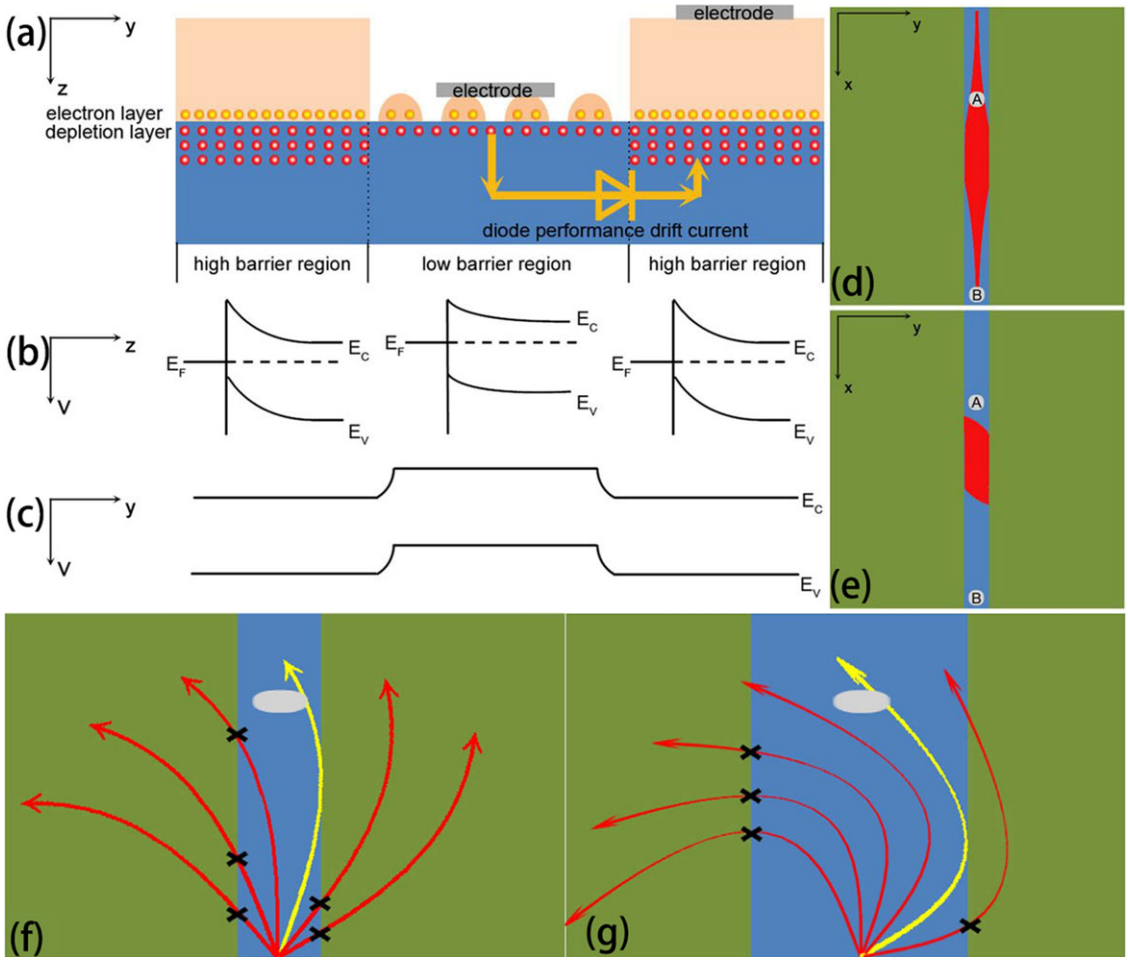

Figure 13. a) Diagram of the carrier distribution in the Cu/SiO_2/n-Si structure. b) Diagrams of energy band of the Schottky junctions. c) The integrated conduction band and valence band of Si layer in y axis. d) Distribution of carriers in the slit area under laser irradiation without magnetic field and e) with high magnetic field. f) Schematic of carrier diffusion in a narrow slit and g) a wide slit under critical magnetic field intensity. Reproduced with permission.[106] Copyright 2019, Springer Nature.

central region is lower than that of the bulk Cu layer as displayed in Figure 13b,c.[107] The lateral field restricts the diffusion of excited holes to the bulk Cu region, and prevents diffusion of electrons into the slit area at the same time. In this premise, the light excited carriers will diffuse only in the x direction (Figure 13d) and when applied with a magnetic field, less carriers reach the electrode away from the laser point due to the obstruction of slit edges and the recombination action (Figure 13e). The density at electrodes significantly decreases but no other carriers can come to compensate, finally inducing the descent of LPV. To deeply investigate this property, schematics are given in Figure 13f,g. When the magnetic field reaches a certain intensity B_c (called as critical magnetic field intensity), the carriers (at laser point) can exactly pass through the right edge like the yellow arrow shown in Figure 13f. Then, as the magnetic field increases, the turning radius of carriers becomes larger (subjected to Lorentz force) and the diffusion would be blocked by the right edge. Thus, the LPV reduces rapidly as soon as the achievement of B_c. Apparently, according to the electromagnetic theories, a wider split will own a larger B_c and permit a bigger turning radius. The interesting results achieved in this special architecture provide a new method to obtain a magnetically susceptible LPE.

Except for the magnetic susceptibility, LPE can also own a temperature dependence in Fe/SiO_2/p-Si structure reported by Volkov et al.[108] As shown in **Figure 14**a, LPV are measured in such structures respectively at Si side (V_{14}) and Fe side (V_{23}), where V_{14} displays a nonmonotonical variation with temperature shown in Figure 14b. Clearly, V_{14} decreases as temperature decreases below 30K. It is mainly because the acceptor levels in p-Si start trapping holes, and makes the number of majority carriers (holes) decrease rapidly. Thus, the semiconductor tends to become intrinsic and the sign of V_{14} changes (red line), which indicates that V_{14} is now dominated by electrons rather than holes and the Schottky field is much weaker than before.[108] The strong decrease of Schottky field means the contribution of concentration diffusion is more significant to V_{14}. In this condition, the photo generated carriers diffuse deeply into Si in concentration gradient (not driven by Schottky field as before) and due

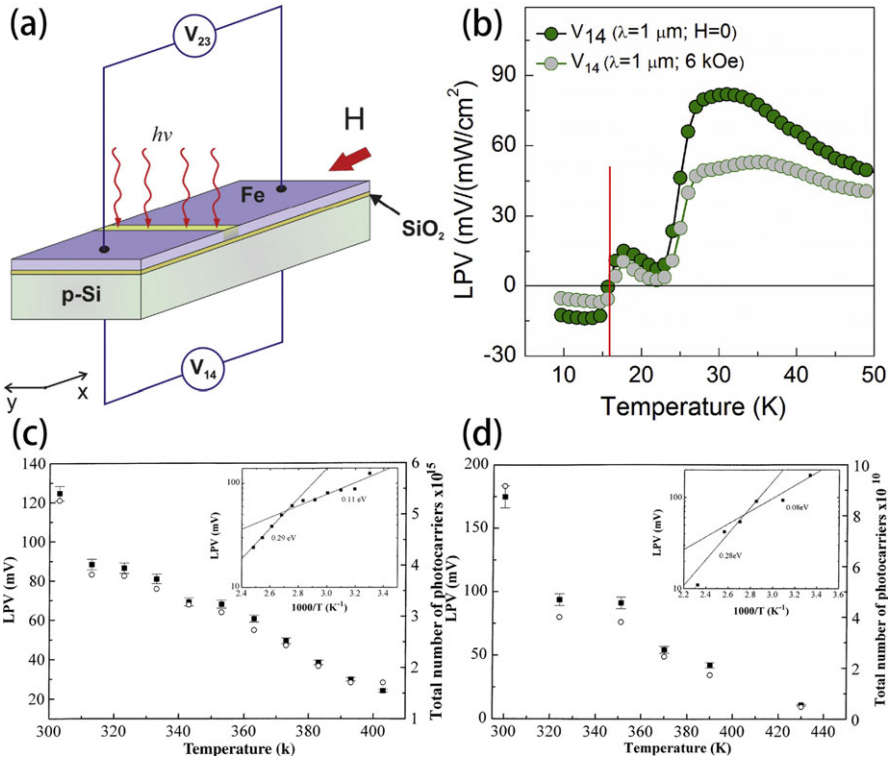

Figure 14. a) Diagram of LPV measurement in Fe/SiO_2/p-Si structure. The voltage measured at Si side is presented as V_{14} and the one measured at Fe side is V_{23} (same contacts in x direction). b) LPV at Si side (V_{14}) as a function of temperature with and without an external magnetic field. The laser of 1 μm and 40 mW cm^{-2} (average power density) is focused in a narrow strip (0.5 mm) fixedly. c) LPV (filled squares) as a function of temperature in the a-Si:H structure. d) LPV (filled squares) as a function of temperature in the a-SiO:H structure. In (c) and (d), right y-axis is the photocarriers (open circles) responsible for corresponding LPV. The laser fixes at 4 mm from the midpoint. Insets are the logarithm of LPV as a function of the reciprocal of temperature. Reproduced with permission.[108,109] Copyright 2019, Elsevier.

to the different diffusivities of electrons and holes, electrons will reach closer to the bottom of Si for owning high mobility. Then, electrons diffuse laterally and induce the LPV. Obviously, the carrier diffusion is much weaker than the carrier drift driven by Schottky field and thus, V_{14} is smaller than it is at high temperature. When the temperature is over 30K, V_{14} decreases as the temperature increases, which can be explained from the view of resistivity. As is known, commonly, resistivity decreases as the temperature increases. According to the LPE theories, in the same external condition, a decline of resistivity will bring a smaller LPV. This statement can also be represented as "an increase in sample conductivity is expected to decrease measured LPV," which is reported by Kodolbas et al. in hydrogenated amorphous silicon (a-Si:H) and hydrogenated amorphous silicon-oxygen (a-SiO:H) structures.[109] The LPV results of a-Si:H and a-SiO:H are shown in Figure 14c,d. The downward tendency with temperature is apparent in both structures and the corresponding conclusion identifies with both the above statements. Judging from the results, the temperature dependence of LPE can be applicative both at low temperature and high temperature. The measuring process is brief and the structures are easy to obtain. Such properties suggest a potential application of LPE in temperature sensor.

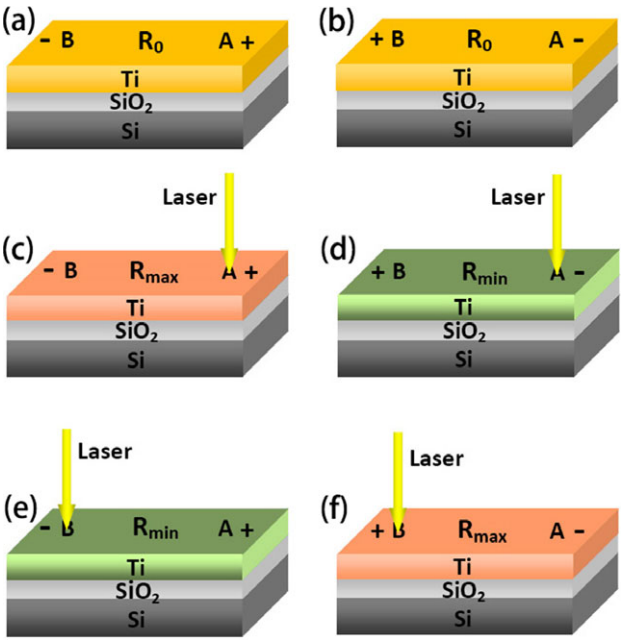

Figure 15. a–f) Schematic of the BRE in Ti/SiO_2/Si structures responding to laser position (632 nm and 3 mW). Reproduced with permission.[119] Copyright 2019, Wiley-Blackwell.

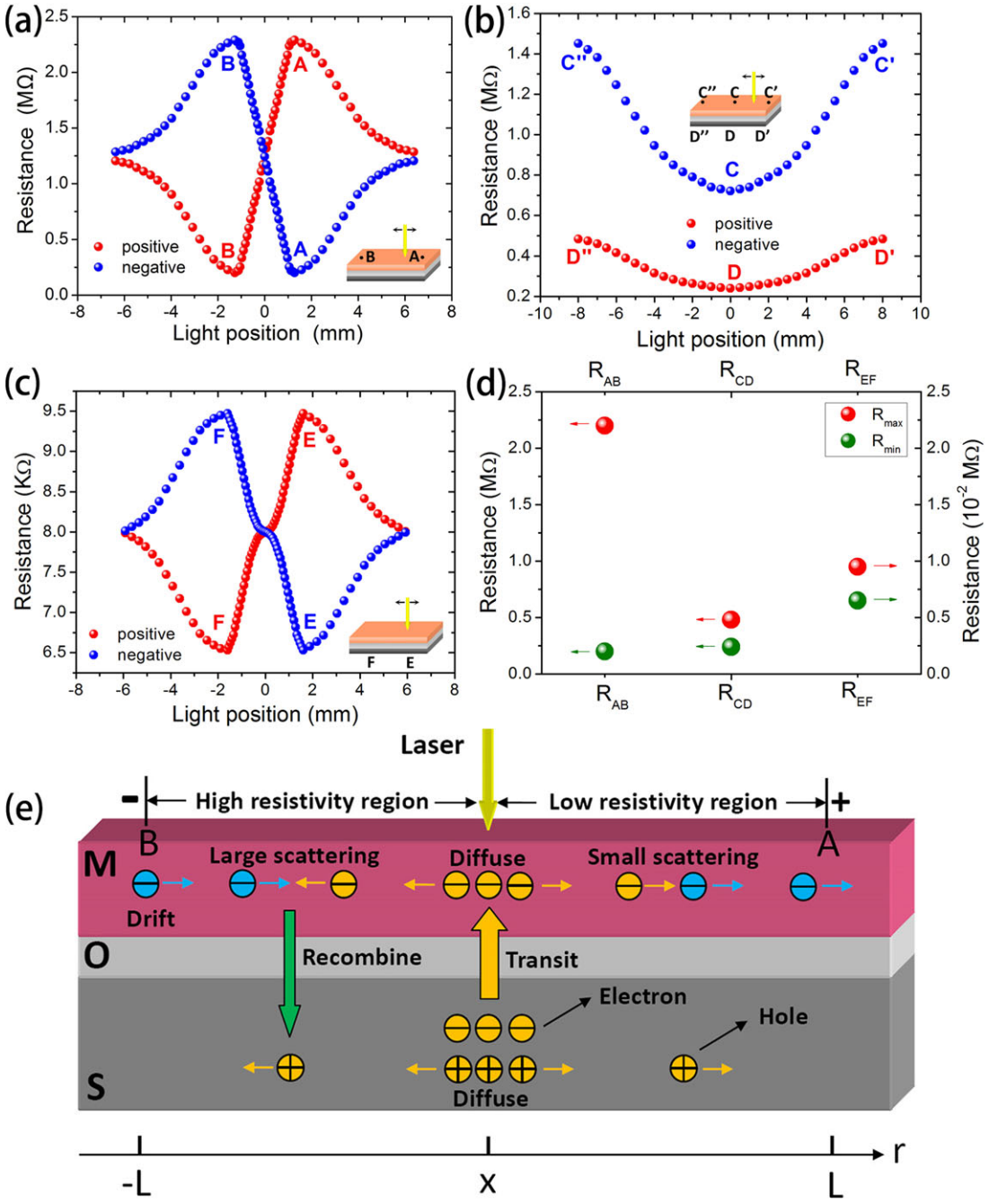

Figure 16. a) Metal side lateral resistance as a function of laser position (632 nm and 3 mW) in a Ti(6.2 nm)/SiO_2/Si structure. The distance between A and B is 2.6 mm. b) Resistance between point C and D as a function of laser position laser position. c) Semiconductor side lateral resistance as a function of laser position. The distance between E and F is 2.6 mm. d) Comparison diagram of R_{AB}, R_{CD}, and R_{EF}. e) BRE schematic in the MOS structure, where the yellow and blue part respectively represent the laser-induced diffusion carriers and drift electrons. Reproduced with permission.[119] Copyright 2019, Wiley-Blackwell.

3. Photo-Induced Resistance Effect

As it turns out, the materials, constructions, and external fields greatly impact the performance of LPE. Moreover, these statements can also apply to resistance effect. Generally, materials' electrical resistance stems from the scattering of electrons and represents a measure of the obstruction to electric current. To date, tremendous efforts have been made on the research of effective manipulation of resistance due to its promising potential in future applications. Although there have existed extensive valuable investigations on resistance effect, such as giant magnetoresistance effect and superconductivity effect,[110–115] new methods for controlling resistance are still in great demand for a briefer operation and a wider range of application. In this section, two

types of resistance effect, including lateral photo-resistance effect and optical switching effect, are presented to exhibit a manipulation of resistance by using laser. Lateral resistance represents the total obstruction in the path of carriers' lateral diffusion to electrodes, containing the scattering and recombination. Section 3.1 exhibits several methods to change part of the obstruction and finally achieves the lateral photo-resistance effect in a controllable manner. Resistance switching means a reversible change between certain metastable states, which is usually stimulated by electric signals. It has drawn plenty of attention due to the huge potential in memory devices.[116–118] Section 3.2 presents some ways to achieve the resistance switching by using optical signals.

3.1. Lateral Photo-Resistance Effect

3.1.1. Optical Bipolar Resistance Effect

Yu et al. has demonstrated an interesting photo-induced resistance effect in MOS systems,[119] which is mainly dominated by the nanosized metal film. As shown in **Figure 15**, a Ti/SiO_2/Si structure is found to have an alterable resistance when irradiated by a laser. Here, the initial metal side lateral resistance (Figure 15a,b) between A and B is 1.2 MΩ (defined as R_0). When point A is irradiated by a laser of 632 nm (3 mW) and measured in mode 1 (A+ B-) as shown in Figure 15c, the lateral resistance increases to 2.2 MΩ (defined as R_{max}). While the laser irradiates on point B as shown in Figure 15e, the lateral resistance decreases to 0.2 MΩ (defined as R_{min}). Inversely, when measured in mode 2 (A− B+), it presents a symmetrical result that R_{min} is 0.2 MΩ (laser on A) and R_{max} is 2.2 MΩ (laser on B) as shown in Figure 15d,f. This phenomenon of tunable resistance with double polarity can be called as "bipolar resistance effect" (BRE).

To learn BRE deeply, a further investigation is given in **Figure 16**. Figure 16a shows the experimental results of lateral resistance response to laser position. Obviously, the curves present a good linearity and a high spatial sensitivity (0.77 $M\Omega^{-1}$). In addition, Figure 16b shows the resistance between point C and D (R_{CD}) response to laser position, where the position-dependent characteristic still exists but the polarity disappears. Figure 16c shows the semiconductor side lateral resistance between point E and F (R_{EF}) response to laser position, where the original resistance is 8 KΩ, R_{max}' is 9.5 KΩ, and R_{min}' is 6.5 KΩ. In this situation, the BRE exists but its performance is not good as previous.

To interpret the mechanism of BRE, a schematic of diffusion model is shown in Figure 16e. When under laser irradiation, large amount of excited electrons generate in semiconductor and transmit to the metal.[120] Then, they will diffuse towards two electrodes away from the laser point. At left region, the excited electrons (yellow dot) diffuse oppositely to the drift electrons (blue dot) driven by external electric field, which results in a large probability of scattering. At right region, these two kinds of electrons diffuse in the same direction, indicating a small probability of scattering. Thus, the left region can be defined as high resistivity region (HR) and the right one is low resistivity region (LR). As the illumination position moves, the length of HR an LR changes,

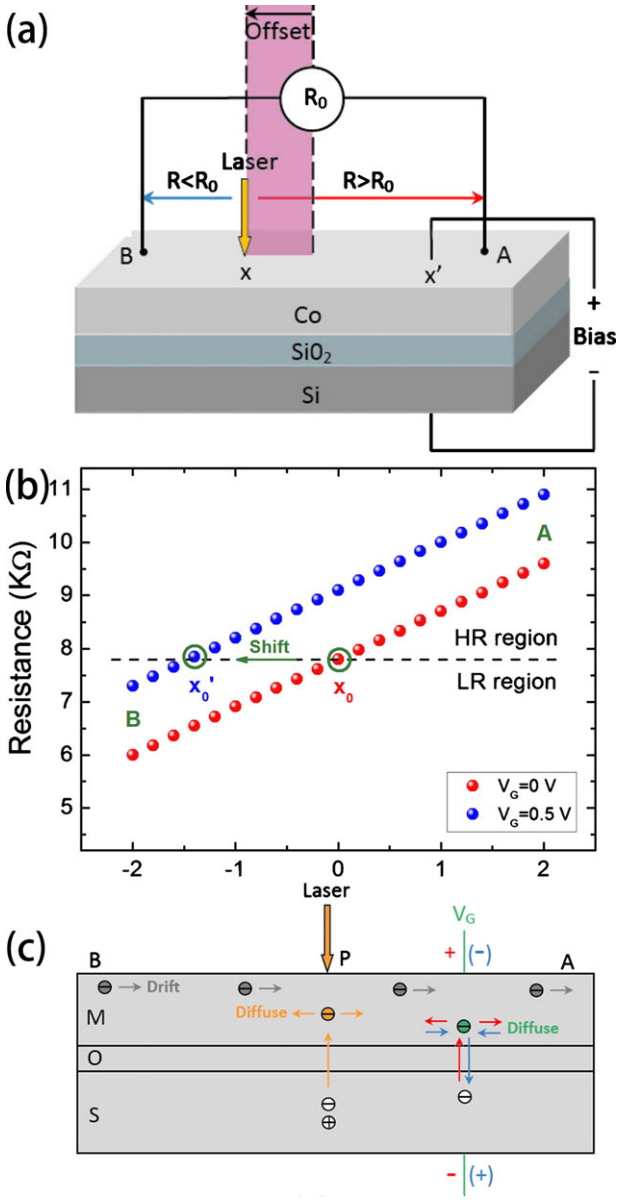

Figure 17. a) Schematic of Co(4 nm)/SiO_2(0.3 nm)/Si(111) structure applied with a bias. The testing mode is (A+ B–). b) Lateral resistance as a function of laser position with different electric bias. c) Schematic mechanism of the voltage bias tuned effect. Reproduced with permission.[123] Copyright 2019, American Institute of Physics.

inducing the variation of total scattering probability and lateral resistance. For example, if the laser point irradiates at $x>0$, the length of HR becomes larger than it of LR and this causes the increase of the resistance. Through a series of calculation, the lateral resistance can be written as

$$R(x) = R_0(1 + Kx)(-L \le x \le L) \tag{11}$$

Where K is a positive coefficient. Thus, if the laser irradiates on position of $x > 0$, $R(x) = R_0(1 + Kx) > R_0$, which is well consistent with previous experimental results.

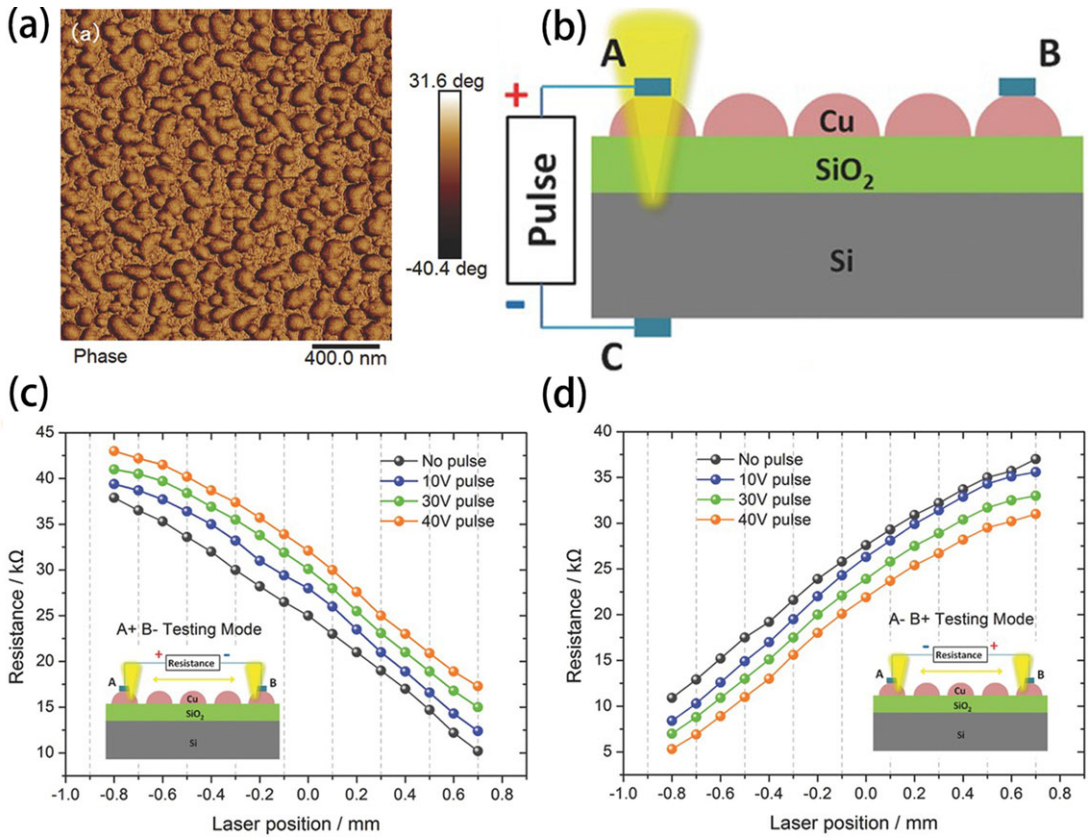

Figure 18. a) Top view of AFM images of the $Cu/SiO_2/Si$ structure with Cu thickness of 2.1 nm. b) Schematic of the measurement applied with a pulse between electrodes and under laser irradiation. c) Under mode 1 and d) model 2, lateral resistance as a function of laser position after applying different electric pulse. Reproduced with permission.[125] Copyright 2019, Wiley-Blackwell.

BRE provides a new method to tune the resistance of MOS systems. Moreover, such characteristic is also observed in other constructions and soon get applied.[121–123] Based on the mentioned structure, a modified $Co(4\ nm)/SiO_2(0.3\ nm)/Si(111)$ structure is built as shown in **Figure 17**a,[123] where the testing mode is (A+ B−) and a longitudinal electric bias is applied at position x' between metal and semiconductor films. In this case, interestingly, the lateral resistance curve with a 0.5 V bias has a clear shift from the one without voltage stimulation (shown in Figure 17b). This means, the resistance has a variation under the action of external voltage and the irradiation position needs an appropriate movement to obtain the original resistance. Here gives a brief explication, in the situation of no electric bias, the model still confirms to ref. [119]. While applied with a vertical voltage, an external group of electrons (green dot) is generated as shown in Figure 17c. These electrons are caused by the fast interface states within the forbidden band due to the formation of SiO_2/Si junction.[124] According to the band theories, when the voltage is positive the external electrons in metal will diffuse laterally toward two electrodes. This action looks like a light irradiating on point x', which enlarge the high resistivity region and induces the increase of total lateral resistance. To obtain the original resistance, the laser point needs a movement away from point x' to offset this enlargement, which is consistent with Figure 17b. Obviously, this new kind of BRE strongly associates the external voltage with the laser position, indicating a photoelectric spatial sensitivity.

3.1.2. Pulse Tuned Photo-Varistor

Sincerely, BRE is very interesting and deserves to be further investigated. Thus, a deeper study is given by Gan et al. using a similar $Cu/SiO_2/Si$ structure.[125] Compared with the structures in refs. [119,123], the major difference here is a thinner Cu film, whose thickness is only 2.1 nm and its particles have a discontinuous distribution on the substrate surface (shown in **Figure 18**a). In this experiment, an electric pulse (between electrode A and C) combined with laser is applied on the $Cu/SiO_2/Si$ structure as shown in Figure 18b. Likewise, the testing modes are defined as mode 1 (A+ B−) and mode 2 (A− B+). After the pulse, the lateral resistance between electrodes (A and B) under laser irradiation is distinct from the one of no pulse stimulated sample. As shown in Figure 18c,d, with the increase of pulse amplitude, the lateral resistance grows in mode 1 and decreases in mode 2. Moreover, as time goes by, the resistance of pulse stimulated samples remains at the excited state, which exhibits that a certain change has occurred in the layered structure.

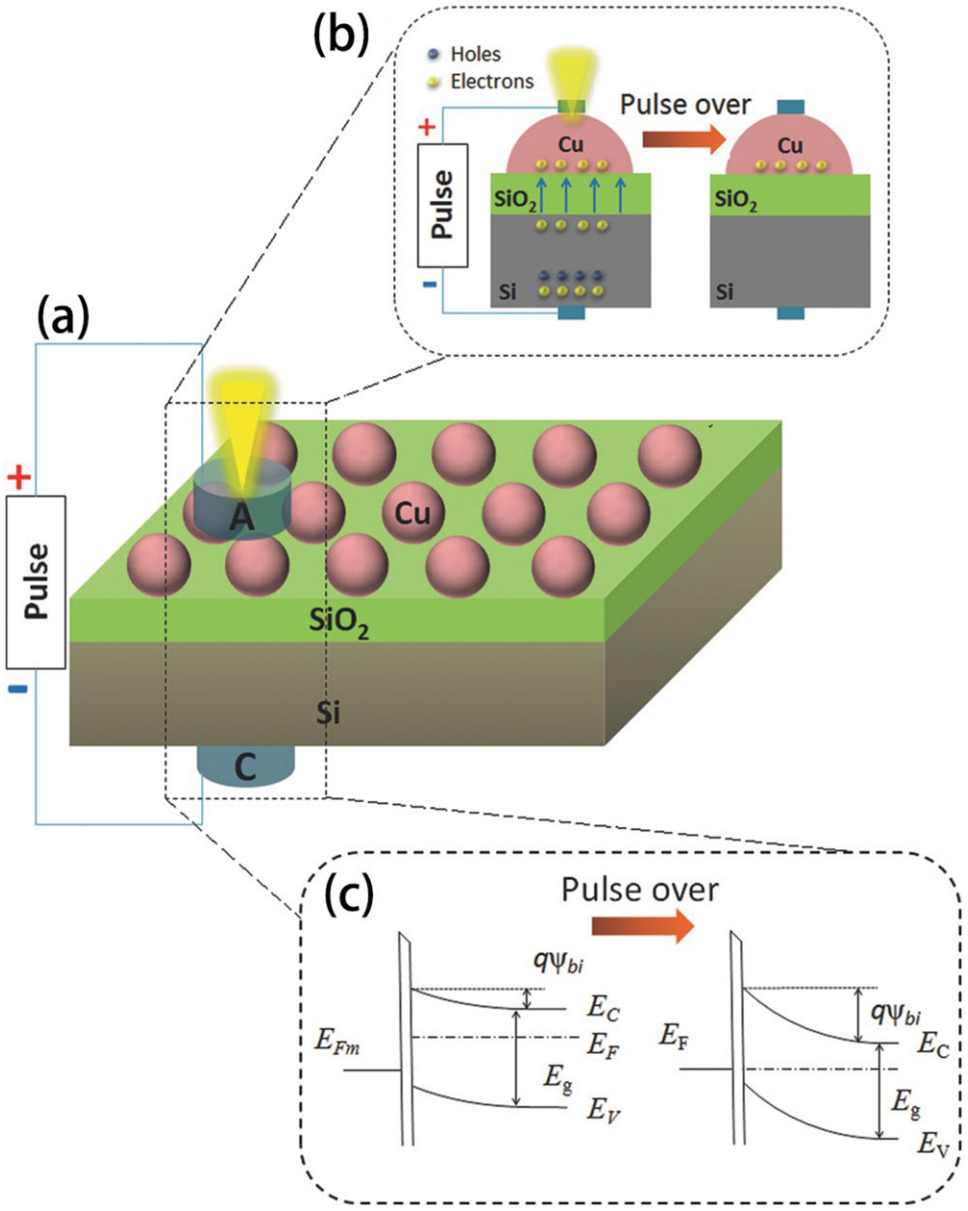

Figure 19. a) Schematic of the measurement under laser irradiation and applied with a forward bias pulse on electrode A. b) Diagram of electron transmitting during and after the pulse. c) Diagram of the energy band during and after the pulse. Reproduced with permission.[125] Copyright 2019, Wiley-Blackwell.

The resistance variation after pulse can be explained as a charge trap effect. When under no pulse stimulation, the lateral resistance also confirms to Equation (11) where the total resistance of $Cu/SiO_2/Si$ structure could be presented as the sum of the barrier resistance, oxide layer resistance, and the resistance of semiconductor between electrodes. However, when applied with a forward bias as shown in **Figure 19**a, the built-in electric field at point A recedes and makes it easier for photogenerated and injected electrons to transmit to the Cu particles (as shown in Figure 19b). Then, after the pulse, the built-in electric field restores to original and obstructs the return of excess electrons in the Cu particles. Due to the discontinuity of the copper layer, the excess electrons are trapped in the Cu side, forming mirror charges and enhancing the built-in electric field (as shown in Figure 19c).[126,127] In mode 1, electrode A is the positive pole and it will collect the electrons when irradiated by a laser. Thus, the larger built-in field after pulse will prevent more electrons from transmitting to electrode A, which induces the increase of the barrier resistance and the whole lateral resistance. Oppositely in mode 2, electrode B is positive pole and the built-in field make it easier for electrons to tunnel from Cu to Si near electrode A, thus decreasing the barrier resistance and the whole lateral resistance. In addition, larger pulse amplitude will bring a larger amount of electrons trapped in Cu particles and lead to a more obvious resistance variation.

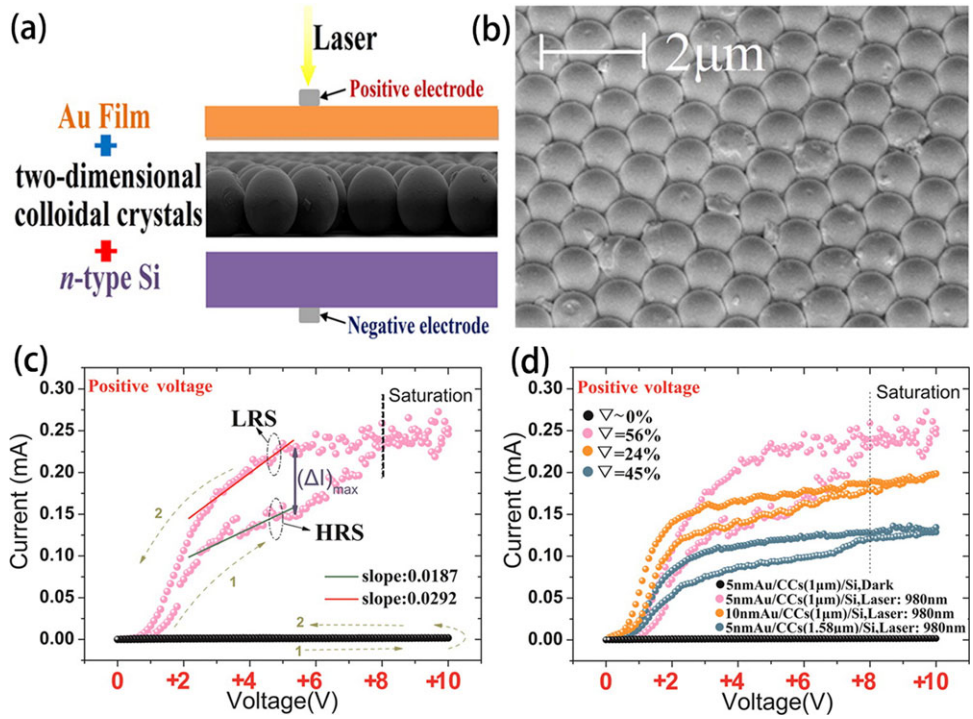

Figure 20. a) Schematic of the measurement in the structure of Au/CCs/Si. b) Top view of SEM images of high ordered two-dimensional CCs whose diameter is about 1 μm. c) I–V curves in the Au(5 nm)/CCs(1 μm)/Si structure irradiated by 980 nm laser and d) I–V curves of this structure with different layer thickness. Reproduced with permission.[129] Copyright 2019, American Chemical Society.

3.2. Optical Switching Effect

Besides the lateral resistance effect, such architectures are also working significantly in the application of longitudinal resistance effect.[128] Liu et al. adds colloidal crystals (CCs) into traditional MS system and observed an interesting property in this novel Au/CCs/Si structure as shown in **Figure 20**a.[129] The layer of CCs makes well-ordered arrays clearly displayed in the SEM images shown in Figure 20b. Usually, for a fixed resistor, there is no difference between the sweeping modes where the voltage is respectively set from 0 to 10 V and 10 V to 0. However, irradiated with a laser of 980 nm, the structure of Au/CCs/Si presents an obvious current hysteresis phenomenon at positive bias region, indicating a latent optical resistance switching effect. In Figure 20c, it can be learned that the positive voltage from 0 to 10 V (step 1) owns a high resistance state (HRS with low conductance G_{HRS}) and oppositely, the one from 10 V to 0 (step 2) owns a low resistance state (LRS with high conductance G_{LRS}). The current disparity reaches the maximum at about +5.5 V and then decreases until saturation. Thus, an additional parameter $\nabla = (G_{LRS} - G_{HRS})/G_{HRS} \times 100\%$ is proposed to give a better description on the resistance properties. Figure 20d presents the I–V curves and their ∇ in different structures, where the most prominent ∇ appears in the structure of Au(5 nm)/CCs(1 μm)/Si and its magnitude reaches 56%. This voltage based resistance is mainly ascribed to the existence of CCs, where abundant oxygen vacancies exist in the microstructure layer. As applied with an external voltage, an oxygen migration occurs and forms conduction filaments between electrodes, which is widely acknowledged as the origin of resistance change.[130] The quantity of conductive filaments built inside CCs layer will grow as increase of external voltage. Thus, there exists more conductive filaments in step 2 due to the higher initial voltage and presents a lower resistance. As for the usage of laser, the photoenergy can greatly increase the density of excited carriers and highlight the changeable resistance. In a manner of speaking, it is the CCs layer that brings this resistance switching effect.

The above work creatively adds the CCs into MS structure and successfully changes its physical properties, which is responsible for the obvious promotion of resistance switching effect under laser irradiation. Here, Lu et al. has also demonstrated a light modulated resistance switching effect in traditional system of n-type Mn-doped $ZnO/SiO_2/Si$ structure.[131] **Figure 21** shows the I–V curves in this structure respectively with different illumination position, different laser power and in dark condition. The results all demonstrate a prominent resistance switching effect under negative bias. Compared with it in dark condition (shown in Figure 21e), when irradiated by a laser on electrode A, the switching voltage shows a remarkable shift dually dependent on the illumination position (shown in Figure 21a) and laser power (shown in Figure 21c). Respectively, while irradiated with a laser of 2 mW, the switching voltage declines with the increase of distance between laser point and electrode A. An enlarged view of the switching region is shown in Figure 21b, it can be seen clearly the switching voltage shifts from −7.4 to −7 V (the switching voltage in dark condition) as the laser point gradually moves away from the electrode. Likewise, while irradiated with a laser fixed nearby electrode A, the switching

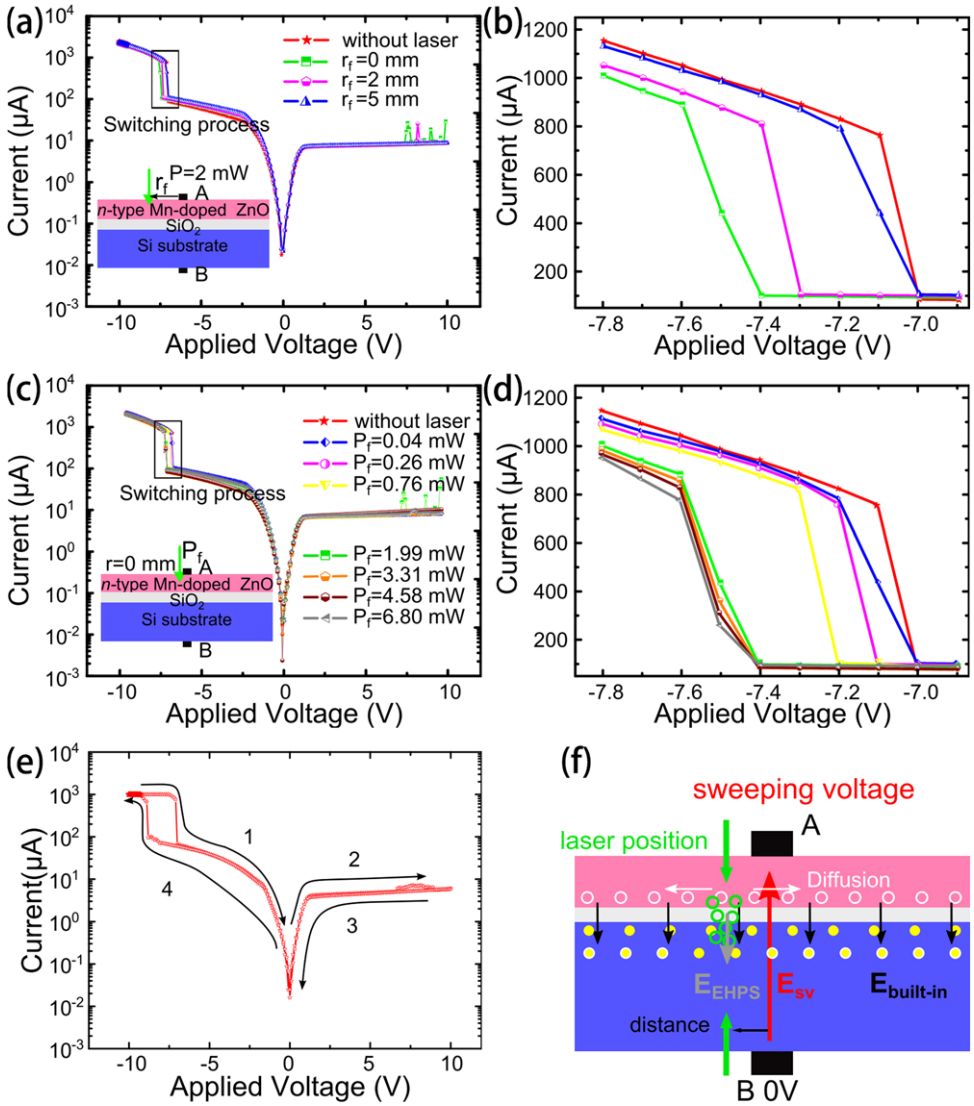

Figure 21. a) I–V curves of the n-type Mn-doped ZnO/SiO_2/Si structure under laser power of 2 mW with different illumination positions. b) Enlarged view of the switching region in (a). c) I–V curves with different power of laser irradiated nearby electrode A. d) Enlarged view of the switching region in (c). e) I–V curves in dark condition. f) Schematic of the switching process under laser irradiation. Reproduced with permission.[131] Copyright 2019, Springer Nature.

voltage rises with the increase of laser power. Related enlarged view shown in Figure 21d displays that the switching voltage reaches the maximum when the power exceeds 2 mW. The resistance switching mechanism here still confirms to the conducting filament model, but when under laser irradiation, a redistribution of photo-generated carriers occurs and alters the electric properties. This optical dual dependence can be explicated through model in Figure 21f. Due to negative bias applied on electrode A, a local electric field (E_{SV}) is formed and it is opposite to the built-in electric field ($E_{built\text{-}in}$). In dark condition, E_{SV} overcomes $E_{built\text{-}in}$ and drives the system to a different resistance state by forming localized conducting filaments.[132] However, when under laser irradiation, the light absorption produces a large amount of electron-hole pairs and finally causes an extra electric field (E_{EHPS}) and a higher internal barrier, which affects the status of conducting filaments. This change of electric properties is responsible for the dual dependence of switching voltage shift. Although the optical enhancement is not large as the structure with CCs, it can regulate the switching characteristics through controlling the irradiation position and laser power, making this traditional structure an outstanding candidate for the future application of resistance switching.

4. Conclusions

In summary, this feature article has presented a review about two certain types of photoelectric effect, LPE, and photo-induced resistance effect. Following the pace of nanoengineering, a detailed discussion is given to exhibit the contributions brought by the nanoscale materials. As demonstrated in the displayed

works, for composite structures, a subtle distinction of microcosmic structure can lead to a prominent variation in the macroscopic results. Especially, the materials' categories and configurations are of great significance to devices' photoelectric performance. For instance, in composite structures, different metal materials will have distinguishing responds to light wavelength which may induce the LPE or resistance effect in diverse degree. An optimum thickness of metal, oxide, and some 2D materials can enhance the LPV greatly and may even induce the charge trap effect. A well-designed architecture may cause a unique phenomenon and boost the photoelectric performance. Besides, the external fields can impact these properties greatly in certain conditions. With the further research, it is sure that LPE and photo-induced resistance effect will perform well because there will be more new kinds of materials and constructions adopted in the experiments. Thus, probably, the detectors and sensors based on LPE can have a faster response time, a wider spectral response and a larger sensitivity. The devices based on photo-induced resistance effect may have a better accuracy, a briefer operation, and a wider range of application. We sincerely hope these effects and MS systems can contribute to the progress of the human society.

Acknowledgements

The authors acknowledge the financial support from the National Natural Science Foundation of China under Grants 61574090, 11874041, 11374214, 10974135, and 60776035.

Conflict of Interest

The authors declare no conflict of interest.

Keywords

lateral photovoltaic effect, metal-semiconductor systems, nanostructures, photoelectric effect, photo-induced resistance effect

Received: October 31, 2018
Revised: January 20, 2019
Published online: March 12, 2019

[1] F. Teng, K. Hu, W. Ouyang, X. Fang, *Adv. Mater.* **2018**, *30*, 1706262.
[2] J. Ke, M. A. Younis, Y. Kong, H. Zhou, J. Liu, L. Lei, Y. Hou, *Nanomicro Lett.* **2018**, *10*, 69.
[3] W. Chen, J. Zhang, G. Xu, R. Xue, Y. Li, Y. Zhou, J. Hou, Y. Li, *Adv. Mater.* **2018**, *30*, 1800855.
[4] M. Hu, Y. Yan, K. Huang, A. Khan, X. Qiu, D. Xu, H. Zhang, X. Yu, D. Yang, *Adv. Opt. Mater.* **2018**, *6*, 1701243.
[5] Z. J. Li, E. Hofman, J. Li, A. H. Davis, C. H. Tung, L. Z. Wu, W. Zheng, *Adv. Funct. Mater.* **2018**, *28*, 1704288.
[6] J. X. Fan, M. D. Liu, C. X. Li, S. Hong, D. W. Zheng, X. H. Liu, S. Chen, H. Cheng, X. Z. Zhang, *Nanoscale Horiz.* **2017**, *2*, 349.
[7] K. Y. Jiang, Y. L. Weng, S. Y. Guo, Y. Yu, F. X. Xiao, *Nanoscale* **2017**, *9*, 16922.
[8] Z. K. Gan, P. Q. Zhou, A. H. Dong, D. Y. Zheng, H. Wang, *Adv. Electron. Mater.* **2018**, *4*, 1800234.
[9] C. Q. Yu, H. Wang, Y. X. Xia, *Appl. Phys. Lett.* **2009**, *95*, 263506.
[10] Z. Huang, W. Zhou, J. Tong, J. Huang, C. Ouyang, Y. Qu, J. Wu, Y. Gao, J. Chu, *Adv. Mater.* **2016**, *28*, 112.
[11] S. Refki, S. Hayashi, H. Ishitobi, D. V. Nesterenko, A. Rahmouni, Y. Inouye, Z. Sekkat, *Ann. Phys.* **2018**, *530*, 1700411.
[12] N. Waiskopf, Y. Ben-Shahar, U. Banin, *Adv. Mater.* **2018**, *30*, 1706697.
[13] A. Jarjour, J. W. Cox, W. T. Ruane, H. Von Wenckstern, M. Grundmann, L. J. Brillson, *Ann. Phys.* **2018**, *530*, 1700335.
[14] A. A. Thahe, H. Bakhtiar, B. A. Ali, Z. Hassan, N. Bidin, M. Bououdina, M. A. Qaeed, Z. A. Talib, M. A. Al-Azawi, H. Alqaraghuli, M. B. Uday, A. Ramizy, M. S. Al-Ghamdi, D. Abubakar, N. K. Allam, *Opt. Mater.* **2018**, *84*, 830.
[15] C. Q. Yu, H. Wang, S. Q. Xiao, Y. X. Xia, *Opt. Express* **2009**, *17*, 21712.
[16] M. V. Schneider, *Bell Syst. Tech. J.* **1966**, *45*, 1611.
[17] M. Ito, O. Wada, K. Nakai, T. Sakurai, *IEEE Electron Device Lett.* **1984**, *5*, 531.
[18] S. Arimoto, H. Yamamoto, *J. Electrochem. Soc.* **1988**, *135*, 431.
[19] R. J. Phelan Jr., J. O. Dimmock, *Appl. Phys. Lett.* **1967**, *10*, 55.
[20] L. A. Dewerd, P. R. Moran, *Med. Phys.* **1978**, *5*, 23.
[21] J. Saghaei, A. Fallahzadeh, T. Saghaei, *Sens. Actuators, A* **2016**, *247*, 150.
[22] L. Aspitarte, D. R. McCulley, E. D. Minot, *J. Appl. Phys.* **2017**, *122*, 134304.
[23] L. Su, W. Yang, J. Cai, H. Chen, X. Fang, *Small* **2017**, *13*, 1701687.
[24] J. M. Halbout, P. Vettiger, W. Patrick, B. J. van Zeghbroeck, *IEEE Electron Device Lett.* **1988**, *9*, 527.
[25] M. Ito, O. Wada, *IEEE J. Quantum Electron.* **1986**, *22*, 1073.
[26] S. Liang, H. Sheng, Y. Liu, Z. Huo, Y. Lu, H. Shen, *J. Cryst. Growth* **2001**, *225*, 110.
[27] J. I. B. Wilson, J. McGill, S. Kinmond, *Nature* **1978**, *272*, 152.
[28] R. J. Stirn, Y. C. M. Yeh, *Appl. Phys. Lett.* **1975**, *27*, 95.
[29] S. J. Fonash, *J. Appl. Phys.* **1975**, *46*, 1286.
[30] W. Rieger, J. J. Heremans, H. Ruan, Y. Kang, R. Claus, *Appl. Phys. Lett.* **2018**, *113*, 023102.
[31] A. R. Peaker, V. P. Markevich, *Mater. Sci. Forum* **2009**, *608*, 181.
[32] F. Zhang, B. Yang, K. Zheng, S. Yang, Y. Li, W. Deng, R. He, *Nanomicro Lett.* **2018**, *10*, 43.
[33] J. He, E. Bi, W. Tang, Y. Wang, X. Yang, H. Chen, L. Han, *Nanomicro Lett.* **2018**, *10*, 49.
[34] F. Huang, A. R. Pascoe, W. Q. Wu, Z. Ku, Y. Peng, J. Zhong, R. A. Caruso, Y. B. Cheng, *Adv. Mater.* **2017**, *29*, 1601715.
[35] Q. M. Thai, N. Pauc, J. Aubin, M. Bertrand, J. Chrétien, A. Chelnokov, J. M. Hartmann, V. Reboud, V. Calvo, *Appl. Phys. Lett.* **2018**, *113*, 051104.
[36] W. Ouyang, F. Teng, M. Jiang, X. Fang, *Small* **2017**, *13*, 1702177.
[37] J. T. Wallmark, *Proc. IRE* **1957**, *45*, 474.
[38] C. Q. Yu, H. Wang, *Opt. Lett.* **2010**, *35*, 2514.
[39] S. Q. Xiao, H. Wang, C. Q. Yu, Y. X. Xia, J. J. Lu, Q. Y. Jin, Z. H. Wang, *New J. Phys.* **2008**, *10*, 033018.
[40] L. Du, H. Wang, *IEEE Electron Device Lett.* **2011**, *32*, 539.
[41] C. Hu, X. Wang, P. Miao, L. Zhang, B. Song, W. Liu, Z. Lv, Y. Zhang, Y. Sui, J. Tang, Y. Yang, B. Song, P. Xu, *ACS Appl. Mater. Interfaces* **2017**, *9*, 18362.
[42] L. Z. Hao, Y. J. Liu, Z. D. Han, Z. J. Xu, J. Zhu, *J. Alloys Compd.* **2018**, *735*, 88.
[43] G. Prestopino, M. Marinelli, E. Milani, C. Verona, G. Verona-Rinati, *Appl. Phys. Lett.* **2017**, *111*, 143504.
[44] J. H. Liu, S. Qiao, B. Liang, S. Wang, G. Fu, *Opt. Express* **2017**, *25*, A166.
[45] C. Zhang, P. Zhu, F. Wang, Y. Ping, J. Wu, Q. Lin, B. Liang, *Appl. Opt.* **2011**, *50*, G127.
[46] X. Huang, C. Mei, J. Hu, D. Zheng, Z. Gan, P. Zhou, H. Wang, *IEEE Electron Device Lett.* **2016**, *37*, 1018.

[47] B. Zhang, L. Du, H. Wang, *Opt. Express* **2014**, *22*, 1661.
[48] X. Huang, C. Mei, Z. Gan, P. Zhou, H. Wang, *Appl. Phys. Lett.* **2017**, *110*, 121103.
[49] B. W. Zhou, Z. K. Gan, A. H. Dong, S. P. Wang, H. Wang, *IEEE Electron Device Lett*. **2018**, *39*, 236.
[50] Z. Gan, P. Zhou, X. Huang, C. Mei, K. Zhang, H. Wang, *Appl. Phys. Lett.* **2016**, *108*, 131111.
[51] S. Liu, H. Wang, Y. Yao, L. Chen, Z. Wang, *Appl. Phys. Lett.* **2014**, *104*, 111110.
[52] A. H. Dong, J. Lu, S. Liu, Z. K. Gan, P. Q. Zhou, H. Wang, *Opt. Express* **2019**, *27*, 743.
[53] A. K. Sarychev, V. A. Shubin, V. M. Shalaev, *Phys. Rev. B* **1999**, *60*, 16389.
[54] K. Seal, M. A. Nelson, Z. C. Ying, D. A. Genov, A. K. Sarychev, V. M. Shalaev, *Phys. Rev. B* **2003**, *67*, 035318.
[55] J. L. Wu, F. C. Chen, Y. S. Hsiao, F. C. Chien, P. Chen, C. H. Kuo, M. H. Huang, C. S. Hsu, *ACS Nano* **2011**, *5*, 959.
[56] S. W. Hwang, D. H. Shin, C. O. Kim, S. H. Hong, M. C. Kim, J. Kim, K. Y. Lim, S. Kim, S. H. Choi, K. J. Ahn, G. Kim, S. H. Sim, B. H. Hong, *Phys. Rev. Lett.* **2010**, *105*, 127403.
[57] P. Cheng, D. Li, Z. Yuan, P. Chen, D. Yang, *Appl. Phys. Lett.* **2008**, *92*, 041119.
[58] J. Lu, Z. Li, G. Yin, M. Ge, D. He, H. Wang, *J. Appl. Phys.* **2014**, *116*, 123102.
[59] J. Henry, J. Livingstone, *J. Phys. D: Appl. Phys.* **2004**, *37*, 3180.
[60] N. Tabatabaie, M. H. Meynadier, R. E. Nahory, J. P. Harbison, L. T. Florez, *Appl. Phys. Lett.* **1989**, *55*, 792.
[61] C. Q. Yu, H. Wang, Y. X. Xia, *Appl. Phys. Lett.* **2009**, *95*, 141112.
[62] C. Yu, H. Wang, *Sensors* **2010**, *10*, 10155.
[63] Z. Gan, B. Zhang, P. Zhou, X. Huang, C. Mei, H. Wang, *Appl. Phys. Lett.* **2016**, *109*, 031106.
[64] K. J. Jin, K. Zhao, H. B. Lu, L. Liao, G. Z. Yang, *Appl. Phys. Lett.* **2007**, *91*, 081906.
[65] G. Lucovsky, *J. Appl. Phys.* **1960**, *31*, 1088.
[66] B. F. Levine, R. H. Willens, C. G. Bethea, D. Brasen, *Appl. Phys. Lett.* **1986**, *49*, 1537.
[67] H. Niu, T. Matsuda, H. Sadamatsu, M. Takai, *Jpn. J. Appl. Phys.* **1976**, *15*, 601.
[68] C. Q. Yu, H. Wang, *Appl. Phys. Lett.* **2010**, *96*, 171102.
[69] S. Liu, X. Xie, H. Wang, *Opt. Express* **2014**, *22*, 11627.
[70] S. Liu, X. Xie, C. Mei, Q. Hu, J. Wang, Q. Zhang, H. Wang, *IEEE Electron Device Lett*. **2018**, *39*, 1393.
[71] L. Chi, P. Zhu, H. Wang, X. Huang, X. Li, *J. Opt.* **2011**, *13*, 015601.
[72] J. Xu, W. Yang, H. Chen, L. Zheng, M. Hu, Y. Li, X. Fang, *J. Mater. Chem. C* **2018**, *6*, 3334.
[73] S. Liu, C. Q. Yu, H. Wang, *IEEE Electron Device Lett.* **2012**, *33*, 414.
[74] S. Qiao, B. Zhang, K. Feng, R. Cong, W. Yu, G. Fu, S. Wang, *ACS Appl. Mater. Interfaces* **2017**, *9*, 18377.
[75] R. Feng, L. Hu, Y. Zhang, M. Zaheer, Z. J. Qiu, C. Cong, Q. Nie, Y. Qin, R. Liu, *Nanophotonics* **2018**, *7*, 1563.
[76] I. K. Moon, B. Ki, S. Yoon, J. Oh, *Sci. Rep*. **2016**, *6*, 33525.
[77] M. Javadi, M. Gholami, Y. Abdi, *J. Mater. Chem. C* **2018**, *6*, 8444.
[78] L. Hao, Y. Liu, Z. Han, Z. Xu, J. Zhu, *Nanoscale Res. Lett.* **2017**, *12*, 562.
[79] J. Schütte, R. Bechstein, P. Rahe, M. Rohlfing, A. Kühnle, H. Langhals, *Phys. Rev. B* **2009**, *79*, 045428.
[80] H. Yang, H. M. Luo, H. Wang, I. O. Usov, N. A. Suvorova, M. Jain, D. M. Feldmann, P. C. Dowden, R. F. DePaula, Q. X. Jia, *Appl. Phys. Lett.* **2008**, *92*, 102113.
[81] D. Kong, H. Wang, J. J. Cha, M. Pasta, K. J. Koski, J. Yao, Y. Cui, *Nano Lett*. **2013**, *13*, 1341.
[82] R. Cong, S. Qiao, J. Liu, J. Mi, W. Yu, B. Liang, G. Fu, C. Pan, S. Wang, *Adv. Sci.* **2018**, *5*, 1700502.
[83] C. Mei, S. Liu, X. Huang, Z. Gan, P. Zhou, H. Wang, *Small* **2017**, *13*, 1701726.
[84] C. Chartier, S. Bastide, C. Lévy-Clément, *Electrochim. Acta* **2008**, *53*, 5509.
[85] X. Li, P. W. Bonn, *Appl. Phys. Lett.* **2000**, *77*, 2572.
[86] Z. Huang, N. Geyer, P. Werner, J. De Boor, U. Gösele, *Adv. Mater.* **2011**, *23*, 285.
[87] Z. Fan, R. Kapadia, P. W. Leu, X. Zhang, Y. L. Chueh, K. Takei, K. Yu, A. Jamshidi, A. A. Rathore, D. J. Ruebusch, M. Wu, A. Javey, *Nano Lett*. **2010**, *10*, 3823.
[88] J. Zhu, Z. Yu, G. F. Burkhart, C. M. Hsu, S. T. Connor, Y. Xu, Q. Wang, M. McGehee, S. Fan, Y. Cui, *Nano Lett*. **2009**, *9*, 279.
[89] C. Mei, J. Zou, X. Huang, B. Zou, P. Zhou, Z. Gan, J. Hu, Q. Zhang, H. Wang, *Nanotechnology* **2018**, *29*, 205203.
[90] S. Zhong, W. Wang, Y. Zhuang, Z. Huang, W. Shen, *Adv. Funct. Mater.* **2016**, *26*, 4768.
[91] M. Yıldırım, A. Kocyigit, *J. Alloys Compd*. **2018**, *768*, 1064.
[92] W. Zhao, Z. Yao, F. Yu, D. Yang, S. F. Liu, *Adv. Sci.* **2018**, *5*, 1700131.
[93] J. Lu, H. Wang, *Opt. Express* **2011**, *19*, 13806.
[94] H. J. Yin, Y. F. Chan, Z. L. Wu, H. J. Xu, *Opt. Lett.* **2014**, *39*, 4184.
[95] K. Zhang, H. Wang, Z. Gan, P. Zhou, C. Mei, X. Huang, Y. Xia, *Sci. Rep.* **2016**, *6*, 22906.
[96] J. M. Luther, P. K. Jain, T. Ewers, A. P. Alivisatos, *Nat. Mater.* **2011**, *10*, 361.
[97] B. Y. Zheng, H. Zhao, A. Manjavacas, M. McClain, P. Nordlander, N. J. Halas, *Nat. Commun.* **2015**, *6*, 7797.
[98] H. Chalabi, D. Schoen, M. L. Brongersma, *Nano Lett*. **2014**, *14*, 1374.
[99] D. W. Boeringer, R. Tsu, *Appl. Phys. Lett.* **1994**, *65*, 2332.
[100] I. Martinez, J. P. Cascales, A. Lara, P. Andres, F. G. Aliev, *AIP Adv*. **2015**, *5*, 117207.
[101] H. Wang, S. Q. Xiao, C. Q. Yu, Y. X. Xia, Q. Y. Jin, Z. H. Wang, *New J. Phys.* **2008**, *10*, 093006.
[102] S. Q. Xiao, H. Wang, Z. C. Zhao, Y. X. Xia, Z. H. Wang, *J. Phys. D: Appl. Phys.* **2008**, *41*, 045005.
[103] L. Z. Kong, H. Wang, S. Q. Xiao, J. J. Lu, Y. X. Xia, G. J. Hu, N. Dai, Z. H. Wang, *J. Phys. D: Appl. Phys.* **2008**, *41*, 052003.
[104] J. Hu, Q. Zhang, P. Zhou, C. Mei, X. Huang, A. Dong, D. Zheng, H. Wang, *IEEE Photonics Technol. Lett.* **2017**, *29*, 1848.
[105] S. Wang, W. Wang, L. Zou, X. Zhang, J. Cai, Z. Sun, B. Shen, J. Sun, *Adv. Mater.* **2014**, *26*, 8059.
[106] P. Zhou, Z. Gan, X. Huang, C. Mei, Y. Xia, H. Wang, *Sci. Rep*. **2017**, *7*, 46377.
[107] S. Doniach, K. K. Chin, I. Lindau, W. E. Spicer, *Phys. Rev. Lett.* **1987**, *58*, 591.
[108] N. V. Volkov, M. V. Rautskii, A. S. Tarasov, I. A. Yakovlev, I. A. Bondarev, A. V. Lukyanenko, S. N. Varnakov, S. G. Ovchinnikov, *Phys. E* **2018**, *101*, 201.
[109] A. O. Kodolbaş, B. Çomak, A. Bacioğlu, Ö. Öktü, *J. Non-Cryst. Solids* **2005**, *351*, 426.
[110] C. N. R. Rao, A. K. Cheetham, *Science* **1996**, *272*, 369.
[111] R. Xu, A. Husmann, T. F. Rosenbaum, M. L. Saboungi, J. E. Enderby, P. B. Littlewood, *Nature* **1997**, *390*, 57.
[112] V. V. Struzhkin, M. I. Eremets, W. Gan, H. K. Mao, R. J. Hemley, *Science* **2002**, *298*, 1213.
[113] A. P. Durajski, R. Szczsniak, L. Pietronero, *Ann. Phys.* **2016**, *528*, 358.
[114] E. F. Talantsev, W. P. Crump, J. G. Storey, J. L. Tallon, *Ann. Phys.* **2017**, *529*, 1600390.
[115] Y. Takagaki, A. Papadogianni, O. Bierwagen, *Adv. Electron. Mater.* **2015**, *1*, 1400007.
[116] M. J. Lee, Y. Park, D. S. Suh, E. H. Lee, S. Seo, D. C. Kim, R. Jung, B. S. Kang, S. E. Ahn, C. B. Lee, D. H. Seo, Y. K. Cha, I. K. Yoo, J. S. Kim, B. H. Park, *Adv. Mater.* **2007**, *19*, 3919.

[117] M. J. Lee, S. Seo, D. C. Kim, S. E. Ahn, D. H. Seo, I. K. Yoo, I. G. Baek, D. S. Kim, I. S. Byun, S. H. Kim, I. R. Hwang, J. S. Kim, S. H. Jeon, B. H. Park, *Adv. Mater.* **2007**, *19*, 73.
[118] H. Y. Yoong, H. Wu, J. Zhao, H. Wang, R. Guo, J. Xiao, B. Zhang, P. Yang, S. J. Pennycook, N. Deng, X. Yan, J. Chen, *Adv. Funct. Mater.* **2018**, *28*, 1806037.
[119] C. Yu, H. Wang, *Adv. Mater.* **2010**, *22*, 966.
[120] R. S. Markiewicz, L. A. Harris, *Phys. Rev. Lett.* **1981**, *46*, 1149.
[121] S. Liu, P. Cheng, H. Wang, *Opt. Lett.* **2012**, *37*, 1814.
[122] T. Lan, S. Liu, H. Wang, *Opt. Lett.* **2011**, *36*, 25.
[123] C. Q. Yu, H. Wang, *Appl. Phys. Lett.* **2010**, *97*, 041105.
[124] D. M. Brown, P. V. Gray, F. K. Heumann, H. R. Philipp, E. A. Taft, *J. Electrochem. Soc.* **1968**, *115*, 311.
[125] Z. Gan, P. Zhou, X. Huang, C. Mei, H. Wang, *Adv. Electron. Mater.* **2017**, *3*, 1700293.
[126] E. Zhang, W. Wang, C. Zhang, Y. Jin, G. Zhu, Q. Sun, D. W. Zhang, P. Zhou, F. Xiu, *ACS Nano* **2015**, *9*, 612.
[127] J. S. Lee, Y. M. Kim, J. H. Kwon, H. Shin, B. H. Sohn, J. Lee, *Adv. Mater.* **2009**, *21*, 178.
[128] P. Zhou, Z. Gan, X. Huang, C. Mei, M. Huang, Y. Xia, H. Wang, *Sci. Rep.* **2016**, *6*, 32015.
[129] S. Liu, M. Huang, Y. Yao, H. Wang, K. J. Jin, P. Zhan, Z. Wang, *ACS Appl. Mater. Interfaces* **2015**, *7*, 19536.
[130] G. Chen, C. Song, C. Chen, S. Gao, F. Zeng, F. Pan, *Adv. Mater.* **2012**, *24*, 3515.
[131] J. Lu, X. Tu, G. Yin, H. Wang, D. He, *Sci. Rep.* **2017**, *7*, 15221.
[132] E. J. Yoo, J. Y. Shin, T. S. Yoon, C. J. Kang, Y. J. Choi, *J. Phys. D: Appl. Phys.* **2016**, *49*, 295109.